THE GEOLOGICAL SOCIETY OF AMERICA®

Petrogenesis of the Cretaceous granitoids in Zhejiang, northeast South China Block and their implications for episodic retreat and roll-back of the Paleo-Pacific Plate

Lu Tao[1,2], Fa-Bin Pan[1,†], Rong Liu[3], Chong Jin[3], Bao-Jian Jia[3], and Xiaobo He[4]

[1]*State Key Laboratory of Geological Process and Mineral Resources, China University of Geosciences, Wuhan 430074, P.R. China*
[2]*Faculty of Earth Science, China University of Geosciences, Wuhan 430074, P.R. China*
[3]*Zhejiang Institute of Geology and Mineral Resource, Hangzhou 310007, P.R. China*
[4]*Ocean College, Zhejiang University, Hangzhou 310058, P.R. China*

ABSTRACT

Two Cretaceous granitoid belts (i.e., the northwest and southeast belts) have been identified in Zhejiang, northeast South China Block. In this study, seven granitoid plutons from both the two belts were collected for zircon U-Pb dating, whole-rock geochemistry, Sr-Nd isotope, and zircon Hf isotope analyses. Chronologically, the Longyou (132 Ma), Sucun (136 Ma), Shanghekou (131 Ma), and Huangshitan (ca. 126 Ma) plutons from the northwest belt display older magma crystallization age than those of the Xiaoxiong (100 Ma), Zhujiajian (108 Ma), and Qingbang island (108 Ma) plutons from the southeast belt. The Sucun quartz monzonite and the Longyou, Shanghekou, Zhujiajian, and Qingbang island granites therein are fractionated I-type granites (i.e., partial melting of meta-igneous rocks) with relatively moderate-low Zr saturation temperature (723–823 °C) and pronouncedly evolved Nd and Hf isotopic compositions ($\varepsilon_{Nd}(t)$ = –8.17 to –5.67 and $\varepsilon_{Hf}(t)$ = –15.07 to –5.67), indicating that they are derivatives of ancient crustal melt-dominated magmas. The Huangshitan granite shows A-type granitic (i.e., granites that are alkaline and anhydrous and from anorogenic setting) features with high Ga/Al (3.47–5.58), rare earth element (REE) content (271–402 ppm), and Zr saturation temperature (781–889 °C). It holds less enriched Nd and Hf isotopic compositions ($\varepsilon_{Nd}(t)$ = –4.13 to –3.60 and $\varepsilon_{Hf}(t)$ = –5.90 to –2.16) and is attributed to partial melting of mature crustal materials with minor basaltic magma incorporation. The Xiaoxiong (quartz) syenitic porphyry is characterized by moderate SiO_2 content (60.68–69.92 wt%), high alkali (9.03–11.66 wt%) and REE contents with fractionated REE pattern [$(La/Yb)_N$ = 13.8–26.1]. Its relatively depleted Nd and Hf isotopic compositions ($\varepsilon_{Nd}(t)$ = –3.67 to –3.42 and $\varepsilon_{Hf}(t)$ = –5.76 to –2.25) imply that it could be a derivative of basaltic magma from K-rich metasomatized mantle. Available geochronological data indicate that there were two episodic magmatic pulses at ca. 140–120 Ma and ca. 110–85 Ma associated with the Paleo-Pacific Plate underthrusting beneath the northeast South China Block. Here we put forward an episodic slab retreat and roll-back model to account for generation of these magmatic rocks. Firstly, the subducting Paleo-Pacific slab roll-back initiated at ca. 140 Ma and reached climax at ca. 130–120 Ma, which led to formation of the Longyou, Sucun, and Shanghekou I-type granites and the Huangshitan A-type granite, respectively. Subsequently, a flat slab subduction stage occurred with eastward trench retreat, causing a period of magmatic quiescence from ca. 120 to 110 Ma. The following second slab roll-back started at ca. 110 Ma and reached climax at ca. 100 Ma, giving rise to the earlier Zhujiajian and Qingbang island I-type granites and the later Xiaoxiong (quartz) syenitic porphyry.

1. INTRODUCTION

The formation and evolution of back-arc basins is one of the most distinctive characteristics in many subduction systems. They are crucial in understanding the development and behavior of subduction zones and their associated mantle geodynamics (Sdrolias and Müller, 2006). It is widely accepted that evolution of back-arc basins are closely correlated with roll-back of subducted oceanic slab (Carlson and Melia, 1984; Schellart et al., 2006; Nakakuki and Mura, 2013) and episodic back-arc extension is confirmed to frequently occur at the West Pacific subduction systems (Schellart et al., 2006; Sdrolias and Müller, 2006). For example, the Izu-Bonin-Mariana subduction system witnessed episodic eastward retreat with sequential opening of the West Philippine Basin, the Parece-Vela Basin, and the Mariana Trough from ca. 55 to 33 Ma (Deschamps and Lallemand, 2002), ca. 30 to 15 Ma (Sdrolias et al., 2004), and ca. 10 Ma to Present (Fryer, 1996), respectively. Similarly, the Tonga-Kermadec subduction system suffered from episodic eastward to northeastward roll-back of the subducting (Paleo-)Pacific Plate from the Late Cretaceous to Cenozoic, leading to successive formation of several back-arc basins (e.g., the New Caledonia Basin, the South Loyalty-Santa Cruz-Pocklington Basin, the South Fiji Basin, the Norfolk Basin, the Lau-Havre Basin, and the Coral Sea) (Schellart et al., 2006; Sdrolias and Müller, 2006). The amounts of eastward roll-back of the Pacific slab during evolution of the South Loyalty Basin, the South Fiji Basin and Norfolk Basin, and the Lau Basin are >1200 km, ~650 km, and ~400 km, respectively (Schellart et al., 2006).

It is worth noting that the South China Block (SCB) experienced subduction of the Paleo-Pacific Plate as early as the early Mesozoic (Zhou et al., 2006; Li and Li, 2007). The subduction-related Mesozoic magmatism, especially the granitoids in the SCB, is various in rock type and widespread in scale (Zhou et al., 2006). Coupling to the large-scale granitoids and their volcanic counterparts, coeval extensional basins are prevalent in the whole Zhejiang Province, northeast SCB. These features indicate that back-arc extension probably occurred during an

†Corresponding author: panfabin@cug.edu.cn.

 https://doi.org/10.1130/B35426.1; 15 figures; 2 tables; Data Repository item 2020026.

early stage of the Paleo-Pacific Plate subduction. If that is the case, the episodic eastward slab rollback with back-arc extension could extend from earlier continental arc stage to later oceanic arc stage for the (Paleo-)Pacific Plate subduction system. To prove this deduction and provide great insights into the behaviors and geodynamic processes of the subduction system, establishing a systemic chronological framework and identifying geochemical and isotopic variations in space and time of the Mesozoic granitoids, together with clarifying distributional characteristics of synchronous extensional basins in the Zhejiang area, is probably an effective way.

The Mesozoic granitoids and their volcanic counterparts with a width of ~1300 km in the SCB are divided into early episode at the early Mesozoic (ca. 251–200 Ma) (Chen and Jahn, 1998; Zhou et al., 2006) and late episode at the middle–late Mesozoic magmatism (ca. 180–67 Ma) (Zhou et al., 2006; Li and Li, 2007). Remarkably, these magmatic rocks not only hold plentiful ore deposits (e.g., W, Sb, Sn, and Bi) (Chen et al., 2014b; He et al., 2017), but also play an important role in deciphering the regional Mesozoic tectono-magmatic evolution. The late episode magmatism shows two intense magmatically active periods of 180–125 Ma and 110–85 Ma and displays a roughly oceanward migration from northwest to southeast (Zhou and Li, 2000; Zhou et al., 2006). They were well-interpreted by flat-slab subduction of the Paleo-Pacific Plate followed by slab roll-back and slab founding (Li and Li, 2007; Jiang et al., 2015). Although this model is coincident with the distribution of the majority of the Mesozoic magmatism in the SCB, it fails to explain the magmatism in the northeast SCB since the following two points: (1) the Mesozoic magmatism in the northeast SCB is relatively narrowly distributed in Zhejiang Province compared to the broad Mesozoic magmatism (i.e., ~1300 km) in the central part of the SCB, and (2) different from the prevalence of the Jurassic magmatism in the central part of the SCB, magmatism in Zhejiang Province is relatively restricted in age spectrum (ca. 145–85 Ma) (Fig. 1C) (Chen et al., 2000; Qiu et al., 2004). Hence, Mesozoic tectonic evolution in the northeast SCB is probably inconsistent with that in the central part of the SCB.

The Mesozoic magmatism in Zhejiang also shows an oceanward younging trend from northwest to southeast (Fig. 1C) (Chen et al., 2000; Qiu et al., 2004; Wong et al., 2009; Li et al., 2013a, 2013b; Chen et al., 2016; Liu et al., 2016; Zhao et al., 2016). Among these igneous rocks, both I- and A-type granitoids are prevalent. Generation of I-type granitoids is usually attributed to subduction of the Paleo-Pacific Plate, whereas emplacement of A-type granitoids could probably rely on an extensional environment (Jahn et al., 1976; Charvet et al., 1994; Lapierre et al., 1997; Wong et al., 2009; Li et al., 2013b). Despite many previous studies of these granitoids, their detailed temporal and spatial distribution, genetic linkage, and the associated geodynamic implications remain ambiguous (Lapierre et al., 1997; Chen et al., 2000; Wong et al., 2009; He and Xu, 2012; Li et al., 2012; Liu et al., 2014; Zhao et al., 2016). Here we report high-precision U-Pb zircon dating, major and trace geochemical, and whole-rock Sr-Nd isotopic and zircon Hf isotopic compositions for seven granitoids from Zhejiang, northeast SCB. Our aims are: (1) to investigate their magma crystallization ages and establish a more detailed chronological framework with available published data, and (2) to discuss the petrogenesis of these granitoids and provide insights into the evolution of the (Paleo-)Pacific Plate subduction system.

2. GEOLOGICAL SETTING

The SCB is separated from the North China Craton by the Qinling-Dabie Orogen, and it is bounded by the Songpan-Ganzi Block and the Tibetan Plateau to the west and by the Philippine Sea Plate to the east (Figs. 1A and 1B). It consists of the Yangtze Block in the northwest and the Cathaysia Block in the southeast (Fig. 1B). The Kongling and Huji areas in western Yangtze Block is characterized by exposure of Archean to Proterozoic basement rocks (Gao et al., 1999; Qiu et al., 2000; Wang et al., 2013; Guo et al., 2015) and the central and southeastern Yangtze Block is considered to have comparable basements (Zheng et al., 2006; Dong et al., 2015), whereas the Cathaysia Block may have a widespread Proterozoic basement (Li et al., 2000; Xu et al., 2007; Yu et al., 2012; Zhao et al., 2014). The two blocks were amalgamated during the early Neoproterozoic (ca. 870–860 Ma) along the 2000-km-long Jiangshan-Shaoxing Fault (JSF) (Li et al., 2008; Li et al., 2009b; Charvet, 2013). After that, the newly formed SCB underwent thick sedimentation and suffered from the early Paleozoic intracontinental orogeny (e.g., Li et al. 2010; Charvet, 2013) until its collision with the Indochina Block at ca. 243 Ma (e.g., Carter et al., 2001) and the North China Craton at ca. 240 Ma (e.g., Ernst et al., 2007).

The NE-SW–trending JSF divides Zhejiang Province into northwest Zhejiang and southeast Zhejiang (Fig. 1C). In northwest Zhejiang, the Shuangxiwu Group is the oldest exposure. It is a sequence of deformed volcanic and sedimentary rocks (Shui, 1988; Li et al., 2009b) that are overlain by the lower Paleozoic strata (Fig. 1C) (Shui, 1988; BGMRZP, 1989). The calc-alkaline volcanic rocks in the Shuangxiwu Group have been interpreted to form in an early Neoproterozoic (ca. 970–890 Ma) continental arc (Shui, 1988; Li et al., 2009b). The Precambrian basement of southeast Zhejiang is composed of the Badu and Chencai groups. The Badu Group dominantly consists of a series of metamorphic terrestrial clastics, including biotite-plagioclase gneiss, amphibolites, amphibole-plagioclase gneiss, biotite-plagioclase-quartz gneiss, mica schist, and mica-quartz schist (Hu et al., 1991). A few granitoids intruded the Badu Group and show Paleoproterozoic emplacement ages of ca. 1.93–1.85 Ga, suggesting a Paleoproterozoic lithostratigraphic unit for their generation (Yu et al., 2012; Zhao et al., 2014; Zhao et al., 2015). The Chencai Group is mainly composed of gneiss, amphibolite, greenschist, and marble (Shui, 1988; Xiao and He, 2005; Li et al., 2009b). Generation of this medium- to high-grade metamorphic complex is likely to represent a relic of the Mesoproterozoic to Neoproterozoic island arc (Shui, 1988).

Widespread Cretaceous extension-related volcanic basins were developed in Zhejiang (Fig. 1C). Cretaceous volcanic-sedimentary sequences from both the northwest Zhejiang and the southeast Zhejiang contain the lower and upper volcanic series. The formation ages of the two volcanic series are ca. 140–118 Ma and ca. 110–88 Ma, respectively (Fig. 2) (Liu et al., 2012; Li et al., 2014). The Jiande Group as the lower volcanic series distributed in the Early Cretaceous basins in northwest Zhejiang contains the Laocun, Huangjian, Shouchang, and Hengshan formations (Fig. 2) (BGMRZP, 1989). The lower part of this group is composed of rhyolites, volcaniclastic rocks, mudstones, and sandstones with volcaniclastic contents decreasing progressively upward. The Qujiang Group, including the Zhongdai, Jinhua, and Quxian formations (BGMRZP, 1989), is the upper volcanic series distributed in the Jinqu and some other small basins in northwest Zhejiang. It contains sandstones, conglomerates, and mudstones with a few interbedded basalts. Correspondingly, the lower volcanic series in southeast Zhejiang, named the Moshishan Group, is widespread in the southeast region of the JSF (Fig. 1C). It contains the Dashuang, Gaowu, Xishantou, Chawan, and Jiuliping formations (Fig. 2) (BGMRZP, 1989). This group mainly consists of rhyolites, volcaniclastic rocks, and minor basalts. The upper volcanic series in southeast Zhejiang is named as the Yongkang Group and Tiantai Group for their distributions in different basins (BGMRZP, 1989; Liu et al., 2012). The Yongkang Group is subdivided into the Guantou, Chaochuan, and Fangyan formations,

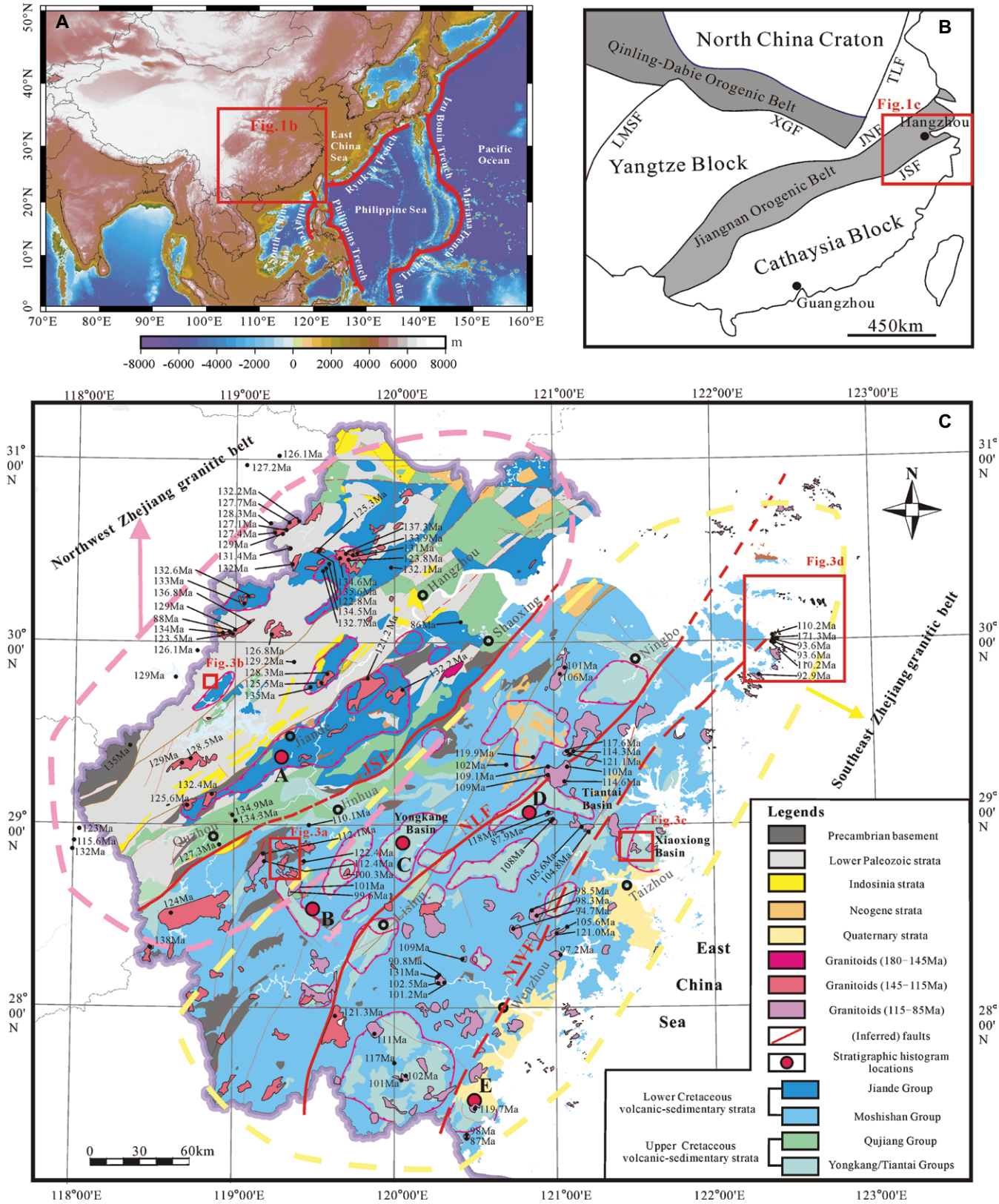

Figure 1. (A) Sketch map showing geological settings of the western Pacific. (B) Tectonic outline of the South China Block. JSF—Jiangshan–Shaoxing fault; JNF—Jiangnan fault; TLF—Tan–Lu fault; XGF—Xiangfan–Guangji fault; LMSF—Longmengshan fault; (C) Simplified geological map of Zhejiang area, northeast South China Block (The detailed age data and data sources are presented in Supplementary Table DR1). NLF—Ningbo-Lishui fault; NWF—Ninghai-Wenzhou fault.

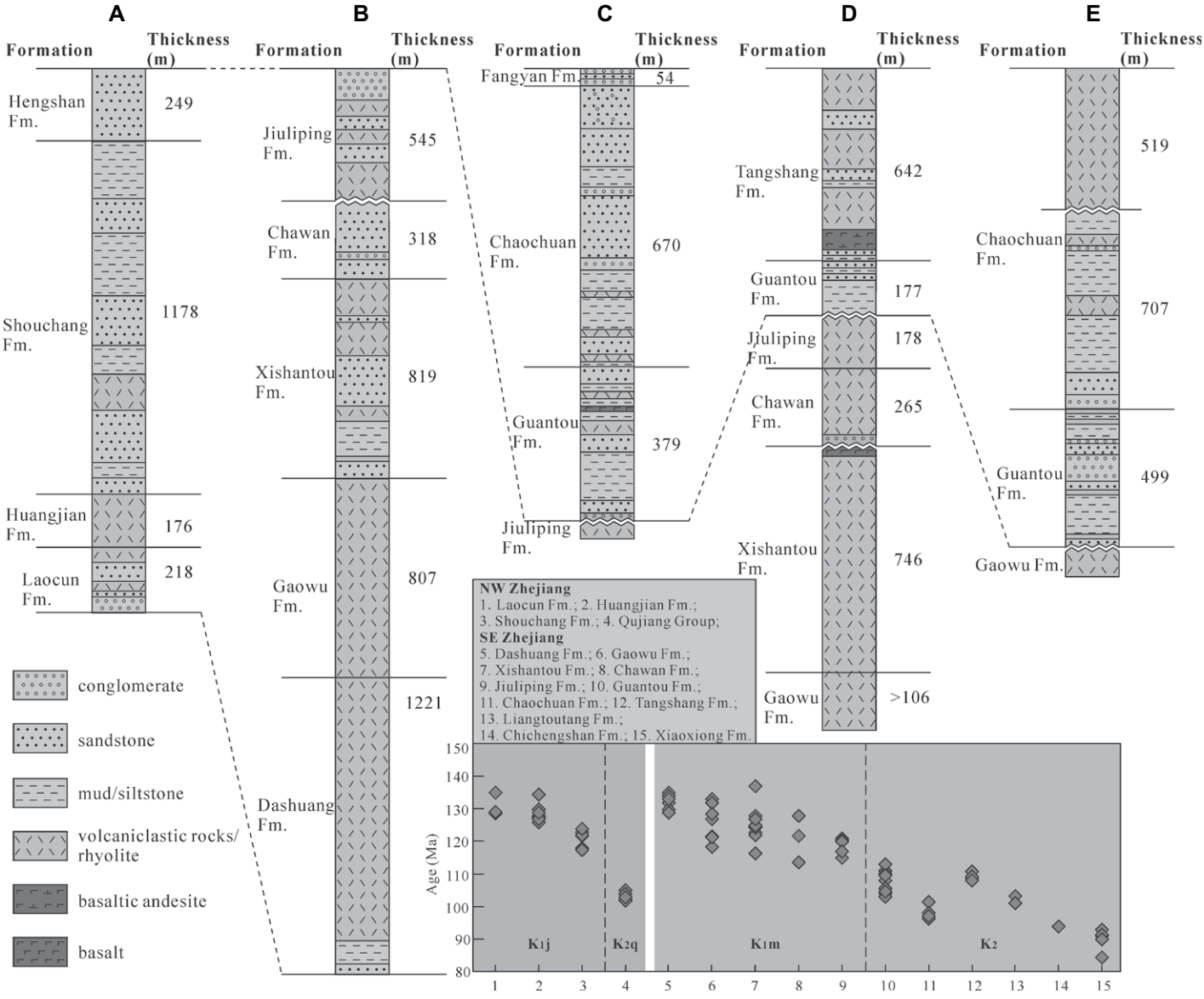

Figure 2. Stratigraphic histograms of the Zhejiang (northeast South China Block) Cretaceous strata showing formation names and ages. The stratigraphic histograms locations are marked in Figure 1C and the age data are from Li et al. (2014), Liu et al. (2012), Liu et al. (2014) and references therein. Fm.—Formation.

while the Tiantai Group consists of the Guantou, Tangshang, Liangtoutang, and Chichengshan formations (Fig. 2) (BGMRZP, 1989). The Xiaoxiong Formation in the Xiaoxiong Basin is considered as the latest volcanic-sedimentary strata of the upper volcanic series and represents the end of the Mesozoic magmatism in the Zhejiang area (He and Xu, 2012). These strata are composed of sandstones, mudstones, and conglomerates with interbedded volcaniclastic rocks, rhyolites, and minor basalts.

Coupled with the extensively distributed volcanics, coeval granitic intrusions are also widespread in the Zhejiang area (Fig. 1C) (Zhou et al., 2006). These granitoids display roughly oceanward younging trend. The proposed ca. 110–85 Ma A-type granitic belt along the coastal Zhejiang area (e.g., Chen et al., 2000; Qiu et al., 2004; Zhao et al., 2016) and coeval I-type granitoids in southeast Zhejiang are called the southeast Zhejiang granitic belt (SE Zhejiang belt) in this study (Fig. 1C). Recently, a few A-type granites (ca. 140–120 Ma) are reported in northwest Zhejiang and adjacent areas (e.g., Wong et al., 2009; Jiang et al., 2011; Yang et al., 2012; Li et al., 2013b; Sun et al., 2015). These A-type granites, together with contemporaneous I-type granitoids in northwest Zhejiang, are named the northwest Zhejiang granitic belt (NW Zhejiang belt) accordingly (Fig. 1C).

3. OCCURRENCE AND SAMPLES

We conducted comprehensive field investigations in the NW and SE Zhejiang belts, respectively. For the former, the Longyou, Sucun, and Shanghekou granitoids were sampled from the northern Suichang city, to the southeast of the JSF, and Huangshitan granite was collected from the northwestern Jiande city, to the northwest of the JSF. For the latter, samples were collected from the Xiaoxiong, Zhujiajian, and Qingbang island, near the Ninghai-Wenzhou fault (Fig. 1C).

The Sucun stock (5.8 km^2) is composed of quartz monzonite and is in sharp contact with

its wall-rocks (i.e., the Badu and Moshishan groups) (Fig. 3A). Among the stock, mafic magmatic enclaves (MMEs) are abundant. They commonly occur as lenses with length of 10–20 cm and show sharp contacts with the host quartz monzonite. The quartz monzonite shows porphyritic texture and comprises quartz, plagioclase, K-feldspar, hornblende, and biotite with subordinate zircon, titanite, apatite, monazite, and Fe-Ti oxides (Fig. 4A). For detailed descriptions of the Sucun quartz monzonite see Pan et al. (2018).

The Longyou pluton (43.8 km^2) is located 5 km to the north of the Sucun pluton (Fig. 3A). The granite is fine- to medium-grained (1–3 mm) and mainly consists of quartz (31–35%), plagioclase (22–25%), K-feldspar (38–42%), and biotite (2–3%) with accessory minerals of zircon, apatite, and Fe-Ti oxides (Fig. 4B).

The Shanghekou pluton (27.5 km^2), ~2 km to the south of the Sucun stock, intruded the Moshishan Group (Fig. 3A). The inner and outer faces of this granite is medium-grained (2–5 mm) and fine-grained (0.5–1.5 mm), respectively. The Shanghekou granite mainly consists of quartz (35–37%), plagioclase (18–20%), K-feldspar (40–45%), and minor biotite (~1%) (Figs. 4C and 4D). Zircon, muscovite, apatite, and Fe-Ti oxides are present as accessory minerals. Zircon inclusions can be observed in some biotites (Fig. 4D).

The Huangshitan pluton that intruded into the Yangliugang Formation has a restricted outcrop area of 1.32 km^2 (Fig. 3B), but regional mapping and interpretation of magnetic and gravity data suggest that it only represents a small part of a huge unexposed pluton (more than 100 km^2, Huang, 2015, personal commun.). Among this pluton, a few biotite granite dykes were emplaced. The Huangshitan granite is medium- to coarse-grained (2–8 mm) and consists of quartz (~35%), plagioclase (~15–20%), K-feldspar (~45%), and biotite (~2%) (Fig. 4E).

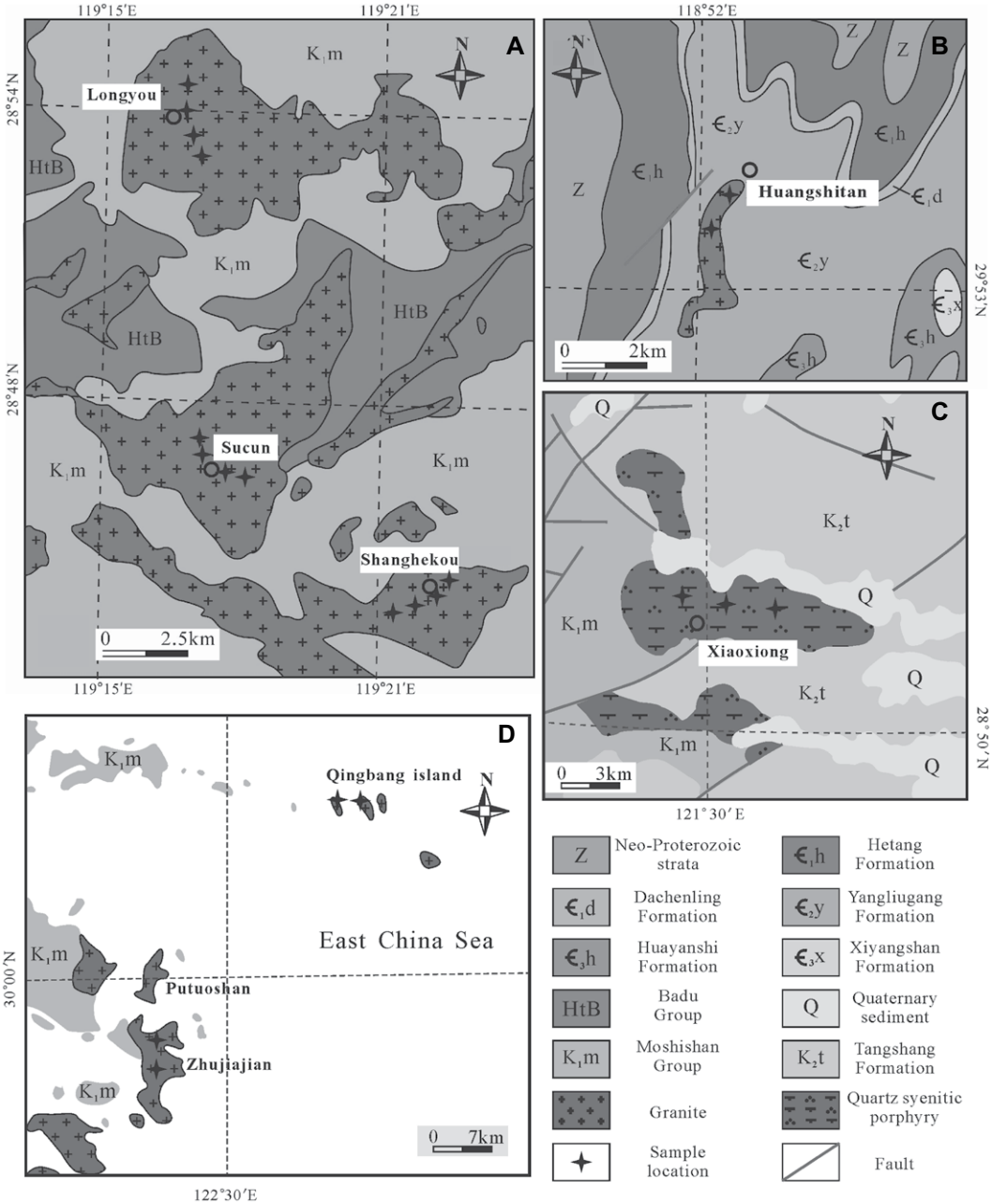

Figure 3. Geological map of the (A) Longyou, Sucun, and Shanghekou plutons, (B) Huangshitan pluton, (C) Xiaoxiong pluton, and (D) Zhujiajian and Qingbang island plutons from Zhejiang, northeast South China Block (modified after 1:200,000 regional geological maps).

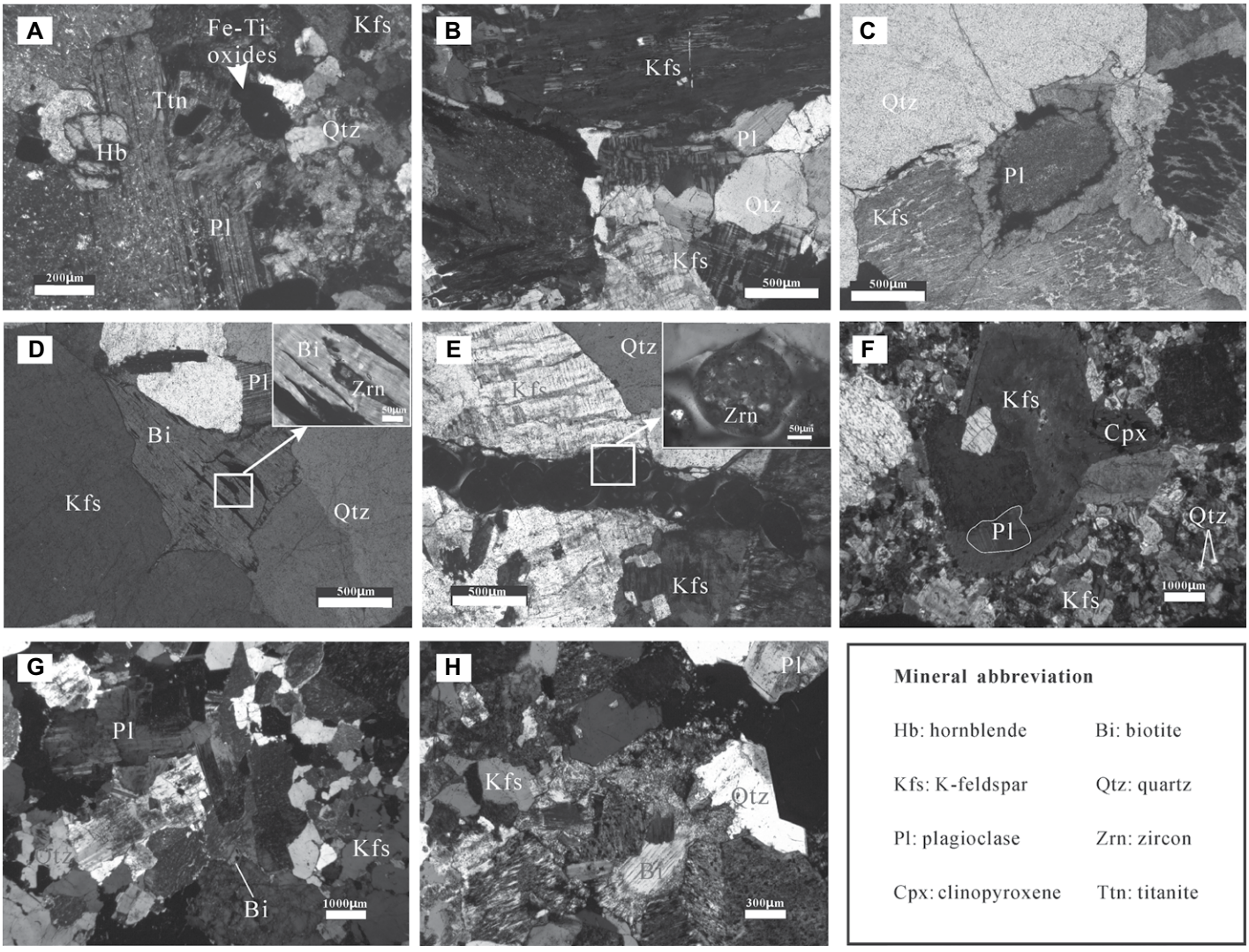

Figure 4. (A) Microphotographs of the Sucun quartz monzonite, (B) Longyou granite, (C and D) Shanghekou granite, (E) Huangshitan granite, (F) Xiaoxiong syenitic porphyry, (G) Zhujiajian granite, and (H) Qingbang island granite from Zhejiang, northeast South China Block.

Accessory minerals therein include zircon, muscovite, apatite, fluorspar, and Fe-Ti oxides. Stringer filled with zircon inclusions could be found in the thin sections (Fig. 4E). One biotite granite sample (HST01) exhibits porphyritic texture with K-feldspar phenocrysts (5–8 mm) comprising ~15–20% of the bulk rock. The remaining matrix (2–4 mm in grain-size) consists of K-feldspar (~40%), plagioclase (~25%), quartz (~30%), hornblende (~2%), and biotite (~3%).

The Xiaoxiong pluton at the Xiaoxiong Basin intruded into the Cretaceous volcanics and is overlain by Quaternary sediments (Fig. 3C). It consists of quartz syenitic porphyry and syenitic porphyry. Both the two lithologies display porphyritic texture. The quartz syenitic porphyry comprises ~25% K-feldspar phenocryst and ~75% matrix (~80% K-feldspar, ~15% quartz, and ~5% biotite) with grain size of 2–7 mm and 0.2–1 mm, respectively. Compared to the quartz syenitic porphyry, the syenitic porphyry is characterized by much less quartz (~2%) and absence of biotite, and the occurrence of plagioclase and clinopyroxene among both the phenocryst and matrix (Fig. 4F).

The Zhujiajian granite outcrops in coastal Zhejiang (Fig. 3D). It is fine to medium with grain size of 1–3 mm and mainly consists of K-feldspar (~45%), quartz (~30%), and plagioclase (~20%) with subordinate biotite (~3%), zircon, and Fe-Ti oxides (Fig. 4G).

The Qingbang island granite to the northeast of the Zhujiajian granite is isolated and small-scale in outcrop (Fig. 3D). It is fine to medium (0.5–2 mm) in grain size. The collected samples mainly consist of K-feldspar (~60%), quartz (~30%) and subordinate plagioclase (~5%), biotite (~2%), zircon, Fe-Ti oxides, and apatite (Fig. 4H).

4. ANALYTICAL METHODS

4.1. Whole-Rock Major and Trace Element Analyses

The fresh samples were first crushed into powder with grain size smaller than 200 mesh for geochemical analyses. Whole-rock major element compositions were analyzed by X-ray fluorescence at the State Key Laboratory of Geological Processes and Mineral Resources (GPMR), China University of Geosciences, Wuhan. The loss on ignition was determined by weight loss after drying at 1000 °C. The

analytical uncertainty is commonly <5%. Trace elements, including rare earth elements (REEs), were measured by Agilent 7500a inductively coupled plasma–mass spectrometer (ICP-MS) at GPMR. For detailed sample-digesting procedures and analytical precision for ICP-MS analysis see Zhang et al. (2017) and Liu et al. (2008), respectively.

4.2. Whole-Rock Sr and Nd Isotope Analyses

Whole-rock Sr and Nd isotopic ratios were also measured at GPMR by a Triton thermal ionization mass spectrometer. Detailed descriptions for sample preprocessing and analytical procedures can be referred to Zhang et al. (2017) and Gao et al. (2004), respectively. $^{87}Rb/^{86}Sr$ and $^{147}Sm/^{144}Nd$ ratios were calculated from Rb, Sr, Sm, and Nd contents measured by ICP-MS. The measured Sr and Nd isotopic ratios were normalized to $^{86}Sr/^{88}Sr = 0.1194$ and $^{146}Nd/^{144}Nd = 0.7219$, respectively.

4.3. Zircon U-Pb Dating and Lu-Hf Isotope Analyses

Zircon grains were firstly selected by a binocular microscope after heavy-liquid and magnetic separation. The chosen zircons were then mounted in epoxy resin and polished to expose their center, after which, cathodoluminescence (CL) images were taken to check their internal textures. Zircon U-Pb dating was then conducted by laser ablation–inductively coupled–plasma mass spectrometry (LA-ICP-MS) at GPMR. Detailed operating conditions are the same as those in Liu et al. (2010). The laser spot is 32 μm in diameter. Reference zircon standard 91500 and DJ-1 with reference ages of 1065.4 ± 0.3 Ma (Wiedenbeck et al., 1995) and 608.5 ± 0.4 Ma (Jackson et al., 2004), respectively, were employed as external standards for Pb/U ratio. NIST SRM610 glass was used as an external standard for elemental content. The measured isotopic and elemental values are displayed as signals in operation interface. Off-line selection and integration of background and analyte signals, quantitative calibration and time-drift correction were conducted by ICPMSDataCal (Liu et al., 2010).

In situ zircon Lu-Hf isotopic analysis was carried out by a Neptune Plus multicollector–inductively coupled plasma–mass spectrometer (MC-ICP-MS) at GPMR. Analytical spots (44 μm in diameter) were chosen close to the U-Pb dating spots or on the same growth domain as shown in CL images. Zircon 91500, GJ-1, and Temora were employed as the reference standard. Detailed analytical method and operating conditions for zircon Lu-Hf isotopic analysis see Hu et al. (2012). Off-line selection and integration of background and analyte signals, and isobaric interference and mass fractionation correction of Lu-Hf isotopic ratios were conducted by ICPMSDataCal (Liu et al., 2010). The decay constant of 1.865×10^{-11} year^{-1} for ^{176}Lu was from Scherer et al. (2001). Initial $^{176}Hf/^{177}Hf$ ratios were calculated at the measured $^{206}Pb/^{238}U$ ages. The $\varepsilon_{Hf}(t)$ values were calculated relative to the chondritic reservoir with $^{176}Lu/^{177}Hf$ and $^{176}Hf/^{177}Hf$ ratios of 0.0332 and 0.282772, respectively (Blichert-Toft and Albarede, 1997).

5. RESULTS

5.1. U-Pb Zircon Ages

All the dated zircons are transparent, subhedral-euhedral, and 100–300 μm in length with aspects ratios of 2:1–3:1. They show typical features of magmatic zircon with clear oscillatory zoning in CL images (Fig. 5). The resultant LA-ICP-MS zircon U-Pb data are listed in Supplementary Table DR2[1] and presented in concordia plots in Figure 6. They are described in two suites corresponding to the different distributions in the NW and the SE Zhejiang belts, respectively.

5.1.1. The Granitoids from the NW Zhejiang Belt

Analyzed zircons from the Longyou granite LY03 have variable U (122–7438 ppm) and Th (84–4915 ppm) contents with high Th/U ratios of 0.29–4.13 (Supplementary Table DR2, see footnote 1 for all supplementary material). Fourteen analyses on zircon crystals yield $^{206}Pb/^{238}U$ ages between 129.0 ± 1.6 Ma and 137.1 ± 3.1 Ma, with a weighted mean of 132.4 ± 1.0 Ma (mean standard weighted deviation [MSWD] = 1.0) (Fig. 6A), representing the magma crystallization age of the Longyou granite. Two additional analyses give $^{206}Pb/^{238}U$ ages of 145.1 ± 2.7 and 145.5 ± 2.0 Ma, which could represent crystallization ages of captured zircons. Another four grains, showing relatively high U (812–7438 ppm) and Th (503–3794 ppm) contents, yield younger $^{206}Pb/^{238}U$ ages between 93.0 and 116.3 Ma (Fig. 6A), which could be due to radiogenic lead loss.

Sixteen analyzed zircons from the Shanghekou granite SHK07 show U content of 195–1749ppm, Th content of 173–1432 ppm, and Th/U ratios of 0.48–1.53. They give $^{206}Pb/^{238}U$ ages between 127.2 ± 2.5 Ma and 137.0 ± 2.7 Ma, with a weighted average of 131.3 ± 1.9 Ma (MSWD = 3.7) (Fig. 6B), representing the magma crystallization age of the Shanghekou granite. Three zircon analyses, exhibiting high U (2403–2642 ppm) and Th (1181–2777 ppm) contents, give younger $^{206}Pb/^{238}U$ ages of 90.8 ± 1.0 Ma, 98.7 ± 0.9 Ma, and 100.1 ± 1.3 Ma, which could result from radiogenic lead loss. One analysis of a captured zircon shows a relatively old age of 144.3 ± 2.8 Ma.

Twenty zircon U-Pb isotopic analyses from the Sucun quartz monzonite SC05 display variable U (151–1265 ppm) and Th (154–1168 ppm) contents with high Th/U ratios of 0.57–1.14. Nineteen analyses yield $^{206}Pb/^{238}U$ ages between 129.7 ± 1.6 Ma and 140.4 ± 2.6 Ma, with a weighted mean of 136.1 ± 1.1 Ma (MSWD = 1.6) (Fig. 6C), representing the magma crystallization age of the Sucun quartz monzonite. One remaining analysis gives $^{206}Pb/^{238}U$ age of 151.6 ± 3.6 Ma, which could represent U-Pb age of a captured grain (not shown in Fig. 6C).

The analyzed zircon grains from the Huangshitan granite HST03 show extremely high U (1754–26926 ppm) and Th (1125–30209 ppm) contents with Th/U ratios of 0.22–1.58. Most of these analyses give discordant $^{206}Pb/^{238}U$ and $^{207}Pb/^{235}U$ ages (Fig. 6D), which could be a consequence of radiogenic lead loss. Five analyses show relatively low U (1754–9689 ppm) and Th (1125–3569 ppm) contents. They yield $^{206}Pb/^{238}U$ ages between 124.5 ± 1.5 Ma and 136.0 ± 2.2 Ma, which are comparable with previously reported age of the Huangshitan granite (i.e., 126 Ma) (Li et al., 2013b). Hence, the age of 126 Ma could be regarded as magma crystallization age of the Huangshitan granite.

5.1.2. The Granitoids from the SE Zhejiang Belt

Fourteen analyses of zircons from the Xiaoxiong quartz syenitic porphyry DSY81 have Th and U contents and Th/U ratios of 209–2966 ppm, 99–876 ppm, and 1.42–3.38, respectively. They display intensive $^{206}Pb/^{238}U$ ages of 97.4 ± 4.8 Ma to 104.1 ± 5.1 Ma, with weighted mean of 100.3 ± 1.6 Ma (MSWD = 0.38) to represent magma crystallization age of the quartz syenitic porphyry (Fig. 6E).

Eleven analyzed zircon grains from the Zhujiajian granite DSY92 show extremely high Th (413–65900 ppm) and U (274–86833 ppm) contents with Th/U ratios of 0.35–2.58. Except for one captured zircon with $^{206}Pb/^{238}U$ age of

[1]GSA Data Repository item 2020026, one supplemental figure to discriminate different types of granites and three supplemental tables presenting both our studied and collected geochronological and isotopic data of granitoids in Zhejiang, northeast South China Block, is available at http://www.geosociety.org/datarepository/2020 or by request to editing@geosociety.org.

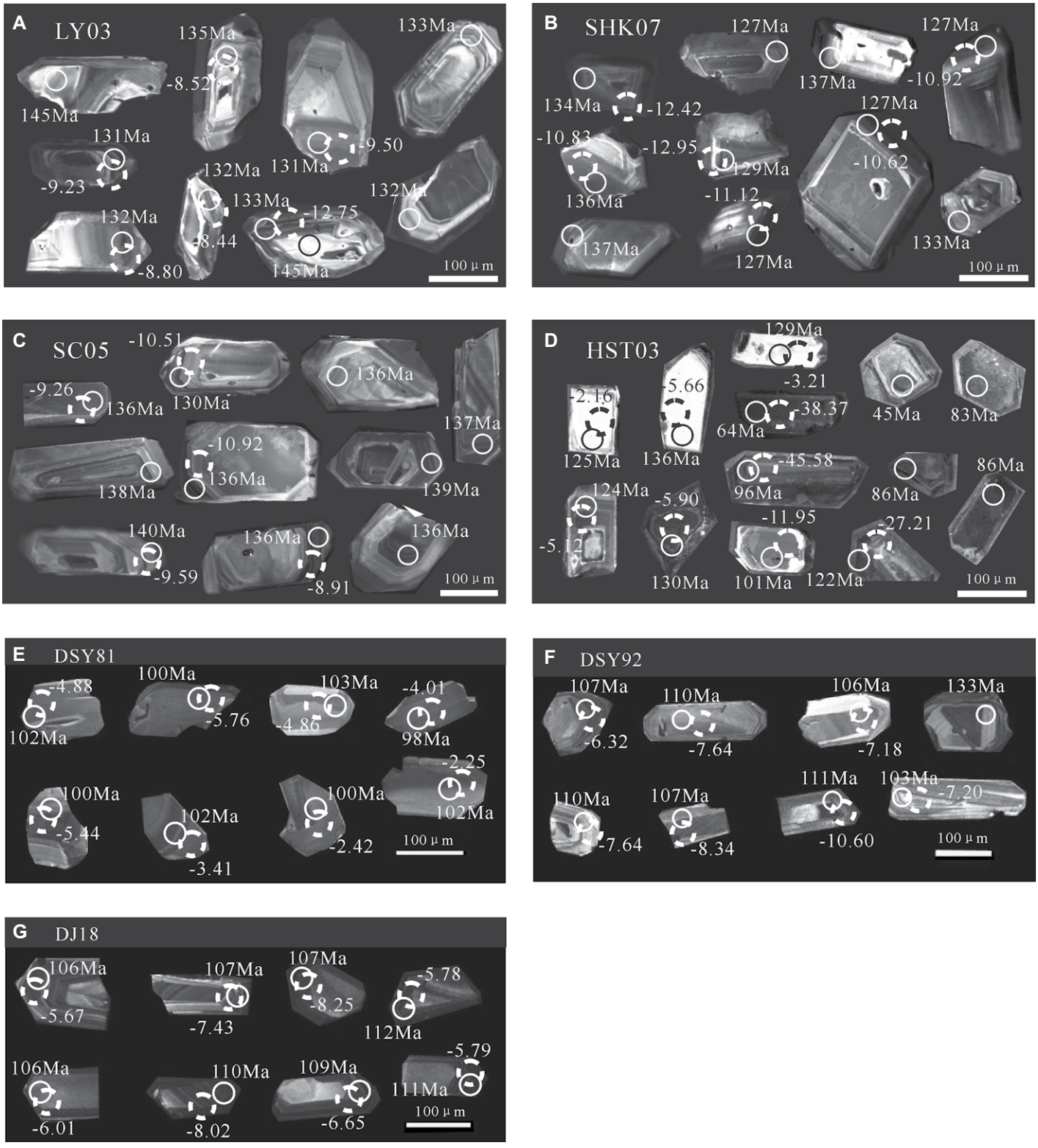

Figure 5. Representative cathodoluminescence images for zircons from samples: (A) Longyou granite sample LY03, (B) Shanghekou granite sample SHK07, (C) Sucun quartz monzonite sample SC05, (D) Huangshitan granite sample HST03, (E) Xiaoxiong syenitic porphyry sample DSY81, (F) Zhujiajian granite sample DSY92, and (G) Qingbang island granite sample DJ18. All the plutons are from Zhejiang, northeast South China Block. The solid circles and numbers show laser ablation–inductively coupled plasma–mass spectrometer dating spots and their corresponding $^{206}Pb/^{238}U$ apparent ages. The dashed circles and numbers are analytical spots of in situ zircon Lu-Hf isotope and $\varepsilon_{Hf}(t)$ values, respectively.

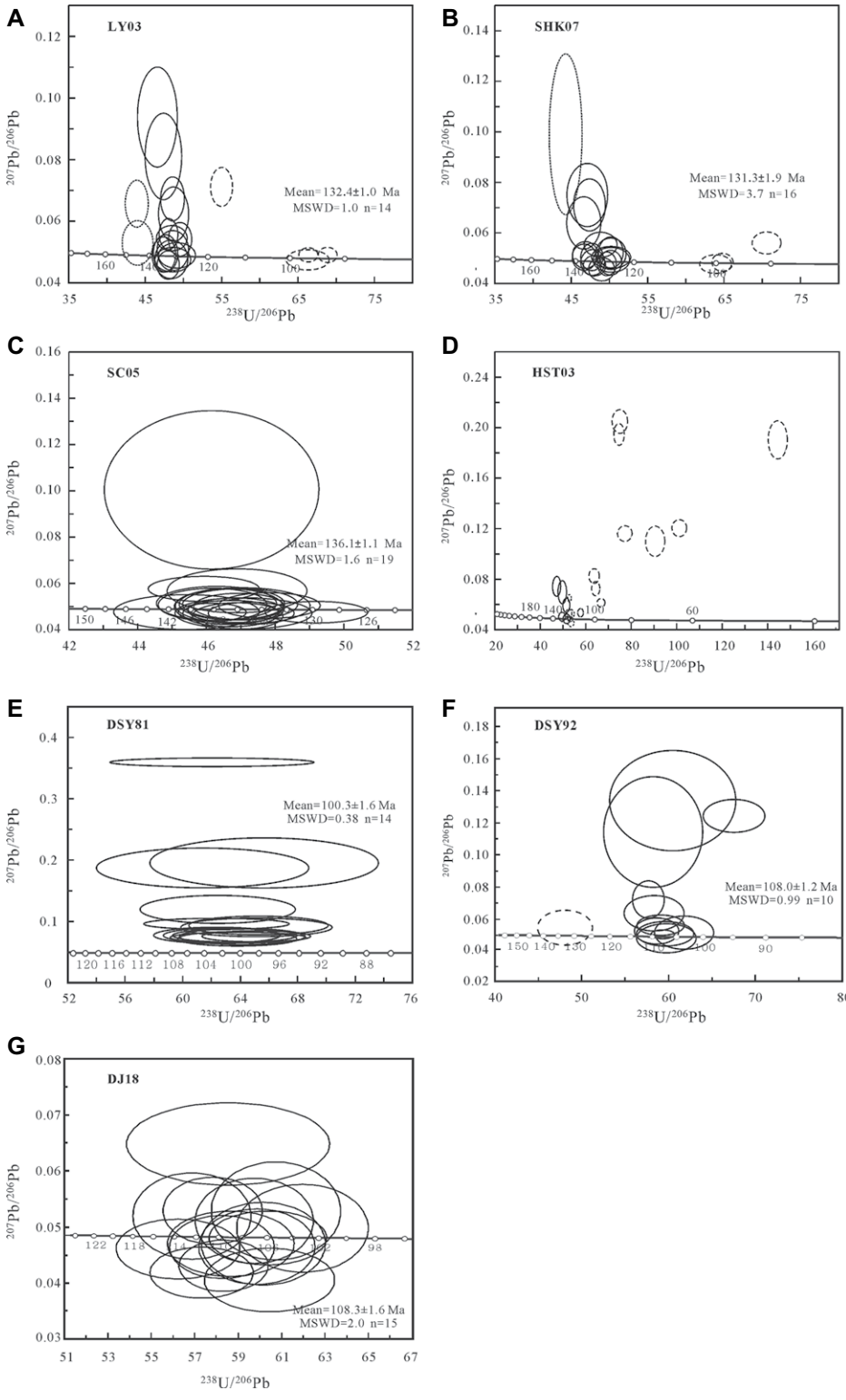

Figure 6. Zircon U-Pb concordia plots for samples: (A) Longyou granite sample LY03, (B) Shanghekou granite sample SHK07, (C) Sucun quartz monzonite sample SC05, (D) Huangshitan granite sample HST03, (E) Xiaoxiong syenitic porphyry sample DSY81, (F) Zhujiajian granite sample DSY92, and (G) Qingbang island granite sample DJ18. All the plutons are from Zhejiang, northeast South China Block. MSWD—mean standard weighted deviation.

132.8 ± 3.6 Ma, the remaining ten analyzed zircons hold intensive $^{206}Pb/^{238}U$ ages of 103.4 ± 2.3 Ma to 110.7 ± 1.5 Ma. Their weighted mean (108.0 ± 1.2 Ma) is employed as magma crystallization age of the granite (Fig. 6F).

Fifteen zircons were analyzed for the selected Qingbang island granite sample DJ18. They display relatively high Th (660–3617 ppm) and U (497–3659 ppm) contents with Th/U ratios of 0.68–1.33. The restricted $^{206}Pb/^{238}U$ ages (103.2 ± 2.1 Ma to 113.6 ± 2.3 Ma) give a weighted mean age of 108.3 ± 1.6 Ma (MSWD = 2.0) (Fig. 6G).

5.2. Major and Trace Elements

In order to characterize the geochemistry of each intrusion, between three and five samples from each intrusion (except for the Xiaoxiong pluton) were analyzed for whole rock major and trace elements. In contrast, eight samples were analyzed for the Xiaoxiong pluton by considering their widely varied lithology. The resultant major and trace elements data of all samples are given in Table 1.

5.2.1. The Granitoids from the NW Zhejiang Belt

Comparing with the Sucun quartz monzonite (SiO_2 = 67.71–68.93 wt%, Al_2O_3 = 14.67–15.03 wt%, TFeO = 3.24–3.57 wt%, MgO = 0.68–0.74 wt%, CaO = 1.57–1.88 wt%, and TiO_2 = 0.44–0.48 wt%), the Huangshitan, Longyou, and Shanghekou granites have higher SiO_2 (70.36–77.41 wt%) and lower Al_2O_3 (11.68–13.47 wt%), TFeO (0.80–1.49 wt%, except HST01 = 4.52 wt%), MgO (0.04–0.58 wt%), CaO (0.51–0.77 wt%), and TiO_2 (0.05–0.19 wt%, except HST01 = 0.59 wt%) contents (Table 1). All the samples from the four plutons are metaluminous to weakly peraluminous (A/CNK = 0.98–1.10, Table 1; Fig. 7B). They exhibit relatively high K_2O content (4.33–5.46 wt%) and K_2O/Na_2O ratio (1.02–1.83), belonging to subalkaline series and lying within the high-K calc-alkaline to shoshonite series field (Figs. 7A and 8A). In the Harker diagrams, samples from each pluton exhibit decreasing trends in MgO, TFeO, Al_2O_3, P_2O_5, and TiO_2 with increasing SiO_2 (Figs. 8B–8F).

All the studied samples show enrichment of Rb, Th, U, and Pb (Fig. 9A). Meanwhile, increasing negative anomalies of Ba, Sr, P, and Ti are observed from the Sucun, Longyou, and Huangshitan plutons to the Shanghekou pluton. Internally, the Huangshitan granite differs from other granitoids by higher Ga and REE contents and Ga/Al ratio (Table 1). In the chondrite-normalized REE patterns (Fig. 9B), the Sucun quartz monzonite displays relatively fractionated REE patterns with $(La/Yb)_N$

TABLE 1. MAJOR ELEMENT (WT%) AND TRACE ELEMENT (PPM) DATA FOR THE STUDIED GRANITOIDS FROM ZHEJIANG, NORTHEAST SOUTH CHINA BLOCK

Pluton	Sucun				Longyou				Shanghekou				Huangshitan		
Sample no.	SC01*	SC04*	SC05*	SC06*	LY01	LY02	LY03	LY04	SHK03	SHK05	SHK06	SHK07	HST01	HST02	HST03
Rock type†	QM	QM	QM	QM	G	G	G	G	G	G	G	G	G	G	G
Major elements (wt%)															
SiO_2	68.11	67.71	68.93	68.35	74.04	75.72	76.37	75.81	76.95	76.39	76.70	75.81	70.36	77.41	76.32
Al_2O_3	14.67	14.79	14.75	15.03	13.47	12.85	12.34	12.78	12.41	12.51	12.73	13.08	13.01	11.68	12.49
TFeO§	3.57	3.43	3.36	3.24	1.49	1.10	1.10	1.04	0.87	1.09	0.80	1.24	4.52	1.27	1.00
K_2O	5.13	5.41	5.13	5.38	5.03	4.80	4.80	5.23	4.43	5.42	4.33	4.68	5.46	4.85	4.63
Na_2O	3.79	3.73	3.63	3.67	3.96	3.88	3.37	3.46	4.17	3.24	4.25	3.71	2.99	3.27	3.81
CaO	1.57	1.63	1.88	1.69	0.77	0.64	0.76	0.62	0.59	0.51	0.56	0.58	0.58	0.71	0.59
MgO	0.74	0.74	0.68	0.71	0.27	0.14	0.17	0.12	0.04	0.09	0.04	0.12	0.58	0.06	0.06
MnO	0.08	0.06	0.09	0.06	0.04	0.04	0.03	0.05	0.03	0.01	0.04	0.04	0.06	0.02	0.02
TiO_2	0.47	0.48	0.44	0.45	0.19	0.13	0.14	0.09	0.05	0.11	0.05	0.10	0.59	0.11	0.07
P_2O_5	0.15	0.16	0.14	0.14	0.05	0.02	0.03	0.01	0.01	0.01	0.01	0.01	0.16	0.01	0.01
LOI	1.72	1.85	0.99	1.28	0.68	0.67	0.90	0.79	0.45	0.62	0.50	0.65	1.69	0.60	1.00
Total	100.00	99.99	100.02	100.00	99.99	99.99	100.01	100.01	100.00	100.00	100.01	100.02	99.99	99.98	100.00
Trace elements (ppm)															
Sc	6.28	6.97	7.03	6.17	2.65	2.03	1.72	1.12	1.60	3.60	1.03	2.74	9.75	1.74	2.43
V	20.6	23.8	20.7	18.5	7.79	4.62	5.38	4.39	1.83	1.84	1.31	1.36	48.9	3.59	2.81
Cr	1.41	1.69	1.28	1.51	0.67	0.59	0.45	0.47	0.92	0.59	0.32	0.41	3.45	0.47	0.40
Co	99.6	71.9	62.5	80.8	118	136	126	122	119	124	117	134	75.1	130	160
Ni	2.25	2.01	1.98	1.81	2.02	2.06	2.27	2.02	2.21	2.17	1.78	2.03	3.33	2.00	2.50
Ga	17.8	18.4	18.5	17.7	18.5	18.6	16.4	16.8	22.1	18.6	20.7	17.6	23.9	27.7	36.9
Rb	184	183	194	191	371	480	434	353	464	323	466	283	263	359	669
Sr	242	236	235	254	96.2	52.7	57.1	72.5	10.7	18.2	5.80	11.1	115	12.4	7.48
Y	34.5	36.1	37.1	31.4	65.1	73.1	57.0	44.8	94.6	52.8	85.2	56.6	56.2	147	164
Zr	265	279	273	247	156	129	131	71.6	151	215	100	116	451	209	148
Nb	20.0	21.1	21.2	17.5	37.8	42.0	37.7	26.1	52.1	29.0	53.2	24.3	29.8	52.9	68.2
Cs	3.97	3.51	3.18	2.75	3.38	4.39	2.66	4.07	2.58	1.87	2.87	2.11	7.74	7.14	9.99
Ba	897	851	770	957	263	159	144	244	21.8	47.7	6.73	19.5	1300	84.9	43.2
La	75.2	77.7	75.7	74.3	39.5	33.6	25.8	39.6	23.8	61.4	9.84	33.0	58.5	79.9	39.2
Ce	136	142	138	134	77.2	66.7	53.2	82.4	57.0	123	27.6	57.8	114	154	86.0
Pr	14.8	15.4	15.1	14.5	9.08	8.47	6.35	9.39	7.64	14.1	4.26	8.42	13.6	17.3	10.6
Nd	53.5	56.7	54.7	51.8	33.9	32.5	24.8	33.3	32.8	53.1	19.9	34.4	54.0	62.4	39.7
Sm	9.23	9.89	10.0	8.85	8.07	8.50	6.19	7.12	10.7	11.5	8.35	8.91	11.0	14.4	11.7
Eu	1.38	1.39	1.29	1.42	0.54	0.33	0.33	0.42	0.080	0.13	0.051	0.15	1.75	0.25	0.070
Gd	7.07	7.52	7.79	6.68	7.34	8.25	5.87	6.12	11.8	9.85	9.68	8.81	9.68	14.3	12.7
Tb	1.09	1.15	1.18	1.00	1.36	1.53	1.15	1.08	2.19	1.56	1.88	1.46	1.55	2.85	2.79
Dy	6.20	6.75	6.93	5.85	9.08	10.4	7.83	6.89	14.6	9.44	12.8	8.83	9.81	20.1	21.0
Ho	1.18	1.28	1.32	1.11	1.89	2.12	1.68	1.43	3.02	1.76	2.69	1.75	1.97	4.27	4.69
Er	3.35	3.50	3.62	3.02	6.21	6.90	5.49	4.55	9.10	4.80	8.06	4.85	5.75	13.2	15.7
Tm	0.50	0.51	0.55	0.43	1.01	1.17	0.95	0.77	1.45	0.75	1.28	0.72	0.89	2.18	2.74
Yb	3.20	3.35	3.41	2.87	7.32	8.20	6.64	5.39	9.98	4.65	9.05	4.70	5.93	14.5	20.6
Lu	0.48	0.47	0.52	0.41	1.19	1.26	1.04	0.86	1.46	0.74	1.32	0.75	0.91	2.08	3.07
Hf	7.23	7.48	7.40	6.78	6.29	5.82	5.93	4.02	8.26	7.96	6.67	5.36	11.7	9.46	10.3
Ta	1.56	1.41	1.46	1.33	5.11	6.56	4.94	5.26	4.38	2.23	4.11	2.19	2.19	4.05	8.20
Tl	0.92	0.83	0.84	0.92	1.49	1.85	1.83	1.58	1.43	1.63	1.78	1.50	1.48	0.84	2.05
Pb	27.7	23.6	23.2	35.1	26.4	33.5	31.2	27.1	47.8	50.3	45.2	32.1	27.6	49.0	73.5
Th	25.7	24.3	25.5	21.9	47.9	50.5	47.1	49.4	67.8	41.9	40.5	32.1	16.9	48.2	55.0
U	3.95	3.72	3.86	2.82	10.6	10.6	14.6	13.6	13.3	8.18	11.7	5.91	4.87	21.2	36.5
$K_2O + Na_2O$	8.92	9.14	8.76	9.05	8.99	8.68	8.17	8.69	8.60	8.66	8.58	8.39	8.45	8.12	8.44
A/CNK#	1.00	0.99	0.99	1.01	1.01	1.01	1.02	1.02	0.98	1.03	1.00	1.07	1.10	0.98	1.01
A/NK**	1.24	1.23	1.28	1.27	1.13	1.11	1.15	1.13	1.07	1.12	1.09	1.17	1.20	1.10	1.11
10000*Ga/Al	2.30	2.35	2.37	2.23	2.59	2.73	2.51	2.49	3.37	2.82	3.08	2.55	3.47	4.47	5.58
ΣREE	313	328	320	306	204	190	147	199	186	297	117	175	289	402	271
Eu/Eu*††	0.50	0.47	0.43	0.54	0.21	0.12	0.16	0.19	0.02	0.04	0.02	0.05	0.51	0.05	0.02
$(La/Yb)_N$	16.9	16.7	15.9	18.6	3.9	2.9	2.8	5.3	1.7	9.5	0.8	5.0	7.1	3.9	1.4
T_{Zr}(°C) §§	820	823	822	814	782	768	772	723	779	817	748	765	889	810	781

(*Continued*)

TABLE 1. MAJOR ELEMENT (WT%) AND TRACE ELEMENT (PPM) DATA FOR THE STUDIED GRANITOIDS FROM ZHEJIANG, NORTHEAST SOUTH CHINA BLOCK (*Continued*)

Pluton	Xiaoxiong								Zhujiajian			Qingbang island				
Sample no.	DSY75	DSY77	DSY78	DSY79	DSY80	DSY81	DSY82	DSY83	DSY92	DSY93	DSY96	DJ1	DJ8	DJ19	DJ17	DJ18
Rock type†	QSP	QSP	SP	SP	QSP	SP	SP	SP	G	G	G	G	G	G	G	G
Major elements (wt%)																
SiO_2	69.68	68.66	60.68	61.50	69.92	64.21	64.08	64.21	75.62	75.77	74.44	76.52	77.11	76.14	75.85	77.08
Al_2O_3	14.28	16.43	16.41	15.81	14.11	16.25	16.55	17.23	13.34	13.05	13.02	12.89	12.57	13.09	13.15	13.05
TFeO§	2.76	1.62	4.81	5.26	2.20	3.16	3.29	2.94	0.58	0.58	1.12	0.58	0.48	0.49	0.58	0.60
K_2O	5.50	5.63	5.21	4.59	5.74	7.27	6.12	8.00	4.32	4.59	4.86	3.80	3.87	4.18	4.20	4.11
Na_2O	3.64	4.71	4.23	4.44	3.85	4.38	5.02	3.58	3.92	3.90	3.50	4.27	4.03	4.11	3.98	4.20
CaO	0.68	0.15	2.24	2.90	0.92	1.12	1.37	0.51	0.40	0.42	0.55	0.31	0.18	0.22	0.28	0.37
MgO	0.42	0.23	1.23	1.45	0.52	0.86	0.77	0.36	0.14	0.13	0.29	0.14	0.12	0.12	0.14	0.13
MnO	0.09	0.03	0.17	0.11	0.09	0.11	0.11	0.04	0.06	0.06	0.03	0.09	0.04	0.04	0.07	0.08
TiO_2	0.65	0.44	1.14	1.30	0.48	0.81	0.84	0.83	0.10	0.09	0.21	0.09	0.08	0.07	0.09	0.09
P_2O_5	0.17	0.05	0.52	0.65	0.10	0.28	0.29	0.28	0.01	0.01	0.04	0.01	0.02	0.01	0.01	0.01
LOI	1.29	1.17	2.41	1.35	1.50	1.23	1.24	1.32	0.60	0.38	0.87	0.56	0.35	0.50	0.44	0.37
Total	99.14	99.12	99.04	99.34	99.43	99.67	99.68	99.30	99.07	99.00	98.92	99.26	98.84	98.98	98.80	100.09
Trace elements (ppm)																
Sc	7.75	6.78	13.0	14.4	7.23	10.0	10.2	9.22	2.87	3.07	3.53	2.80	2.06	2.77	2.54	2.55
V	18.9	10.9	54.5	64.6	12.5	20.3	23.2	23.7	2.32	1.90	9.26	1.18	2.42	1.16	1.75	1.53
Cr	0.85	0.55	1.06	0.72	2.02	1.38	0.48	0.93	0.29	0.45	0.47	0.15	0.52	0.54	0.25	0.79
Co	1.53	0.54	5.83	7.01	0.76	1.30	1.31	0.68	0.22	0.96	0.55	0.098	0.33	0.081	0.11	0.16
Ni	0.47	0.49	1.89	1.93	1.30	1.22	0.43	0.76	0.20	0.51	0.36	0.11	0.27	0.34	0.16	0.55
Ga	20.0	20.5	21.7	22.9	21.5	21.3	22.7	22.8	15.4	16.2	15.5	19.0	16.2	18.0	16.4	16.4
Rb	154	131	85.9	60.9	128	185	119	226	227	220	216	271	253	285	192	192
Sr	109	118	280	325	49.5	131	138	115	22.9	23.3	107	37.3	10.1	15.3	16.0	6.47
Y	41.6	52.3	45.1	41.7	42.2	37.1	37.6	59.2	14.0	15.9	17.7	42.5	24.9	38.0	28.5	29.4
Zr	481	497	489	487	600	459	518	525	74.3	82.1	160	95.1	73.2	92.1	93.5	84.2
Nb	26.7	26.8	17.8	16.8	24.8	16.3	17.9	16.9	17.3	17.2	17.4	34.3	26.5	34.6	26.0	23.5
Cs	4.70	1.42	1.75	1.02	2.31	2.74	2.55	2.87	3.92	3.77	2.49	2.69	2.55	1.90	1.37	1.13
Ba	1117	691	1733	2056	228	1851	1847	1907	69.1	87.2	376	24.7	19.7	11.5	21.7	14.2
La	83.0	157	106	111	118	109	121	120	21.8	25.9	51.2	18.4	12.0	14.0	16.8	18.4
Ce	161	250	195	215	227	209	223	230	41.5	44.4	87.5	40.4	28.4	27.3	31.7	38.4
Pr	18.1	30.7	22.9	23.4	24.9	23.3	25.0	29.2	3.98	4.63	8.29	4.68	3.01	3.55	3.94	4.43
Nd	67.1	108	87.9	90.1	89.1	86.4	93.5	119	11.6	14.0	26.1	16.9	10.7	12.6	14.0	15.8
Sm	11.7	17.8	15.1	14.7	14.3	13.9	15.2	19.9	1.94	2.23	3.92	4.48	2.96	3.55	3.56	3.80
Eu	2.39	2.60	4.32	4.34	1.75	3.98	4.18	5.23	0.20	0.26	0.54	0.15	0.16	0.13	0.23	0.24
Gd	8.94	12.6	11.3	11.1	9.61	9.63	10.5	15.1	1.64	1.78	2.77	4.56	2.91	3.65	3.38	3.61
Tb	1.31	1.92	1.57	1.50	1.43	1.33	1.43	1.99	0.29	0.31	0.44	0.88	0.56	0.71	0.64	0.66
Dy	7.51	10.1	8.54	7.91	8.14	7.28	7.49	10.6	1.80	2.02	2.69	6.10	3.72	4.98	4.15	4.32
Ho	1.45	1.86	1.60	1.47	1.52	1.28	1.40	2.01	0.40	0.45	0.55	1.31	0.78	1.10	0.87	0.92
Er	4.14	5.05	4.10	4.03	4.16	3.37	3.60	5.27	1.32	1.43	1.64	4.10	2.26	3.32	2.60	2.76
Tm	0.65	0.78	0.60	0.55	0.64	0.49	0.52	0.73	0.24	0.25	0.27	0.65	0.41	0.54	0.45	0.46
Yb	4.31	5.06	3.85	3.55	4.14	3.03	3.33	4.38	1.76	1.88	2.04	4.61	2.68	3.89	3.06	3.18
Lu	0.65	0.74	0.56	0.52	0.61	0.45	0.50	0.61	0.28	0.29	0.33	0.65	0.39	0.57	0.43	0.46
Hf	10.9	12.1	9.21	9.50	12.1	8.58	9.60	9.59	3.18	3.66	4.81	4.71	3.46	4.52	4.03	3.42
Ta	1.58	1.45	0.98	0.94	1.43	0.89	0.96	0.91	1.19	1.23	1.15	2.57	1.91	2.44	1.84	1.69
Tl	0.75	0.63	0.38	0.44	0.45	1.61	0.83	1.76	0.95	0.95	1.03	1.86	1.34	1.31	0.76	0.67
Pb	28.4	30.7	22.2	20.3	25.2	19.5	20.3	18.0	23.9	22.7	18.2	32.9	26.3	24.2	39.1	23.4
Th	14.7	14.1	6.90	6.71	11.4	5.54	6.14	5.79	23.7	23.9	30.2	32.8	23.6	31.8	21.2	20.1
U	3.38	2.64	1.52	1.27	2.33	0.96	1.17	1.13	4.06	6.40	4.33	4.32	4.73	5.32	3.86	3.49
$K_2O + Na_2O$	9.13	10.34	9.44	9.03	9.59	11.66	11.13	11.58	8.23	8.49	8.35	8.08	7.90	8.30	8.18	8.31
A/CNK#	1.08	1.17	0.98	0.90	0.99	0.95	0.95	1.11	1.13	1.07	1.08	1.10	1.13	1.12	1.13	1.09
A/NK**	1.20	1.19	1.30	1.29	1.12	1.08	1.11	1.18	1.20	1.15	1.18	1.16	1.16	1.16	1.19	1.15
10000*Ga/Al	2.65	2.36	2.50	2.74	2.87	2.48	2.59	2.50	2.18	2.35	2.26	2.78	2.44	2.60	2.36	2.37
ΣREE	372	605	464	489	505	473	511	564	89	100	188	108	71	80	86	98
Eu/Eu*††	0.69	0.50	0.97	1.00	0.43	1.00	0.96	0.89	0.34	0.38	0.48	0.10	0.16	0.11	0.20	0.19
$(La/Yb)_N$	13.8	22.3	19.7	22.5	20.4	25.9	26.1	19.7	8.9	9.9	18.0	2.9	3.2	2.6	4.0	4.2
T_{Zr}(°C)§§	892	901	862	849	904	855	868	893	734	738	794	752	734	753	741	751

Note: LOI—loss on ignition.

*Data from Pan et al. (2018).

†Rock type abbreviations: G—granite, QM—quartz monzonite, SP—syenitic porphyry, and QSP—quartz syenitic porphyry.

§TFeO = all Fe calculated as Fe_2O_3.

#A/CNK = $Al_2O_3/(CaO + Na_2O + K_2O)$molar.

**A/NK = $Al_2O_3/(Na_2O + K_2O)$molar.

††Eu/Eu* = $2*Eu_N/(Sm_N+Gd_N)$.

§§Zr saturation temperature [T_{Zr}(°C)] calculated after Watson and Harrison (1983) and Miller et al. (2003).

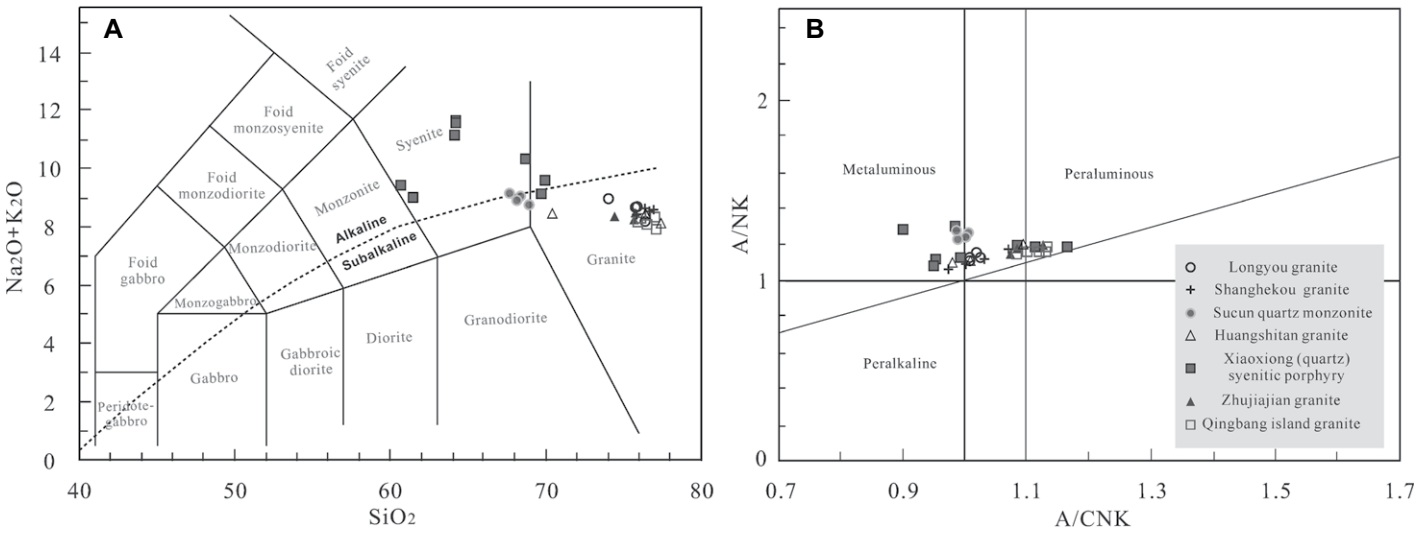

Figure 7. Plots of (A) total alkali versus silica (after Middlemost, 1994) and (B) A/NK versus A/CNK (after Maniar and Piccoli, 1989) for the studied granitoids from Zhejiang, northeast South China Block.

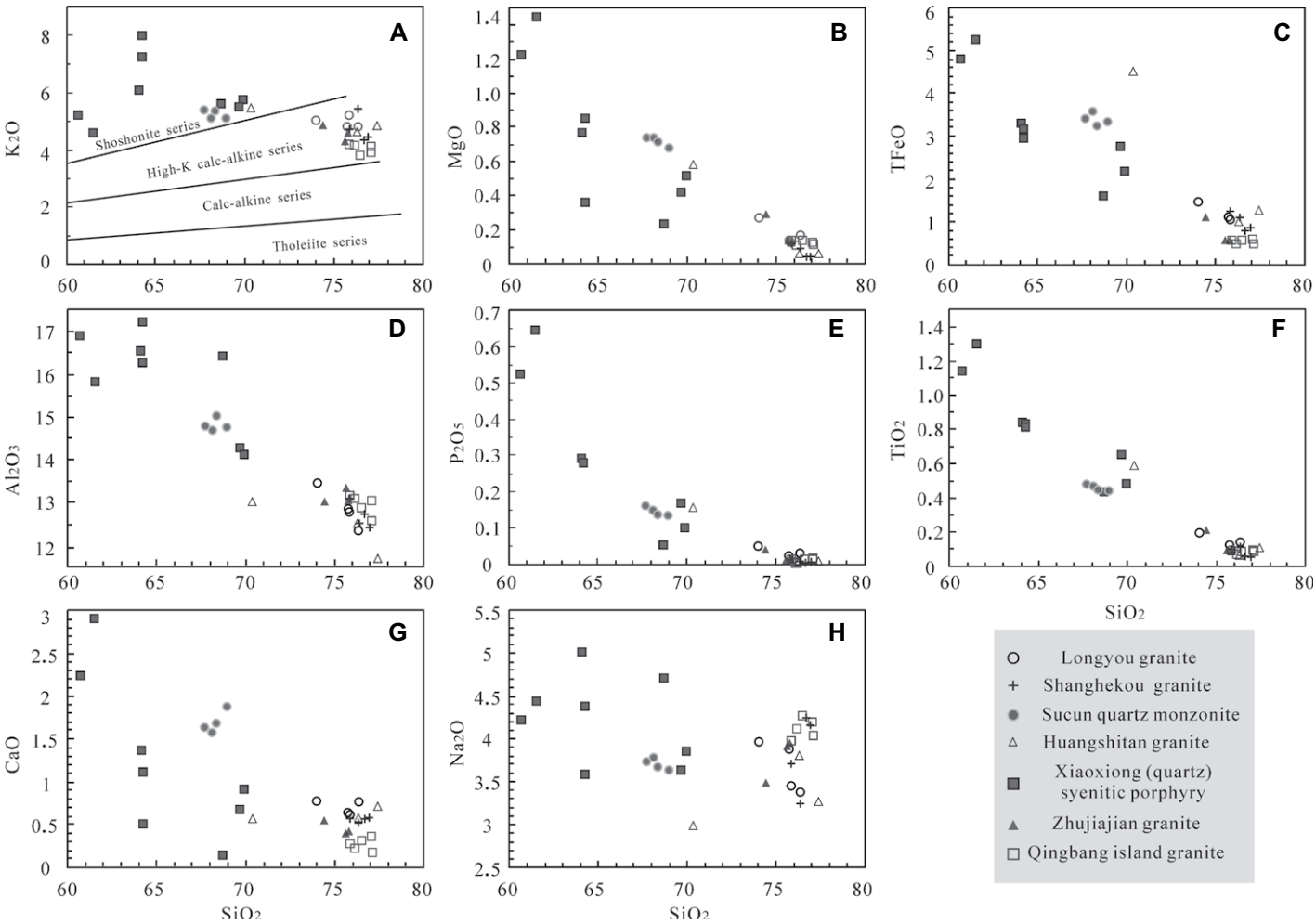

Figure 8. Harker diagrams for the studied granitoids from Zhejiang, northeast South China Block.

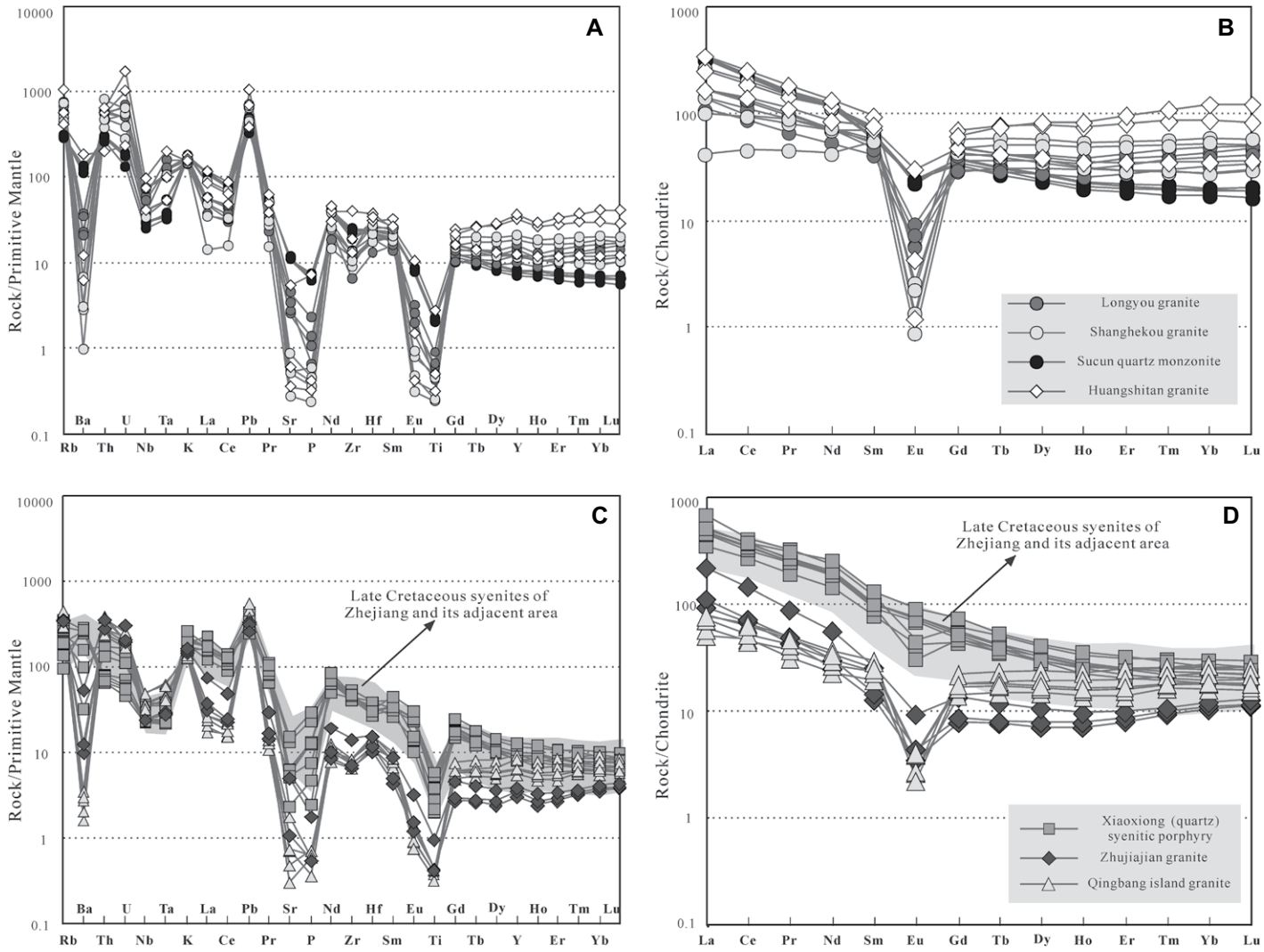

Figure 9. (A and C) Primitive mantle-normalized element spider diagrams and (B and D) chondrite-normalized rare earth element patterns for the studied granitoids from Zhejiang, northeast South China Block. Normalizing values are from Sun and McDonough (1989). The Late Cretaceous syenites of Zhejiang and its adjacent area from Li and Jiang (2014) and He and Xu (2012) and references therein.

ratios of 15.9–18.6 with negative Eu anomalies (Eu/Eu* = 0.43–0.54), whereas the Longyou, Huangshitan, and Shanghekou granites display weakly fractionated REE patterns with $(La/Yb)_N$ ratios of 0.8–9.5 with more strongly negative Eu anomalies (Eu/Eu* = 0.02–0.21, except HST01 = 0.51).

5.2.2. The Granitoids from the SE Zhejiang Belt

The samples from the Xiaoxiong pluton are widely varied in SiO_2 content (60.68–69.92 wt%). They have relatively high Al_2O_3 (14.11–17.23 wt%), TFeO (1.62–5.26 wt%), and TiO_2 (0.44–1.30 wt%) and extremely high K_2O (4.59–8.00 wt%) and Na_2O (3.58–5.02 wt%) contents, belonging to the shoshonite series (Fig. 8A). By contrast, those granites from the Zhujiajian and Qingbang island plutons have restricted SiO_2 (74.44–77.11 wt%) and Al_2O_3 (12.57–13.34 wt%), low TFeO (0.48–1.12 wt%) and TiO_2 (0.07–0.21 wt%), and moderate K_2O (3.80–4.86 wt%) and Na_2O (3.50–4.27 wt%) contents, which makes them fall into the high-K calc-alkaline field. On the A/CNK versus A/NK diagram, both the Zhujiajian and the Qingbang island granites are weakly-strongly peraluminous with A/CNK = 1.07–1.13, while samples from the Xiaoxiong pluton vary from metaluminous to strongly peraluminous with A/CNK = 0.90–1.17 (Table 1; Fig. 7B). Negative correlations are observed between SiO_2 and MgO, TFeO, P_2O_5, TiO_2, and CaO for the Xiaoxiong and Zhujiajian plutons (Figs. 8B, 8C, and 8E–8G). In addition, K_2O and Al_2O_3 are firstly increasing and then decreasing with increasing SiO_2 for the Xiaoxiong pluton (Figs. 8A and 8D).

In the trace element spider diagram (Fig. 9C), the Zhujiajian and Qingbang island granites show enrichment of Rb, Th, U, and Pb and negative anomalies of Ba, Sr, P, Nb, Ta, and Ti. They have weakly-moderately fractionated REE patterns ($(La/Yb)_N$ = 2.6–18) and moderately-strongly negative Eu anomalies (Eu/Eu* = 0.10–0.48) (Fig. 9D). By contrast, the Xiaoxiong (quartz) syenitic porphyries display no obvious depletion of Ba and less depletion of Sr, P, and Ti, but they show negative anomalies of Nb and Ta. All the samples are characterized by high REE concentrations. In the REE spider diagram (Fig. 9D), they show strongly fractionated REE patterns with $(La/Yb)_N$ ra-

tios of 13.8–26.1 and no obvious to weakly negative Eu anomalies (Eu/Eu* = 0.43–1.00).

5.3. Whole-Rock Sr-Nd Isotopes

Whole-rock Rb-Sr and Sm-Nd isotopic data for the granitoids are listed in Table 2 and plotted in Figure 10. For all the samples, their initial $^{87}Sr/^{86}Sr$ isotopic ratios [i.e., $(^{87}Sr/^{86}Sr)_i$] and $\varepsilon_{Nd}(t)$ values are calculated at their magma crystallization ages.

For the studied granitoids in the NW Zhejiang belt, the Longyou granites have $(^{87}Sr/^{86}Sr)_i$ of 0.7033–0.7078 and $\varepsilon_{Nd}(t)$ values of –7.99 to –7.58, with two-stage Nd depleted mantle model age (T_{2DM}) values of 1.5–1.6 Ga. The Shanghekou granites have variable $(^{87}Sr/^{86}Sr)_i$ ranging from 0.6634 to 0.7102 and $\varepsilon_{Nd}(t)$ values ranging from –8.08 to –7.67, with T_{2DM} values of 1.5–1.6 Ma. For the Sucun quartz monzonites, they show restricted $(^{87}Sr/^{86}Sr)_i$ and $\varepsilon_{Nd}(t)$ values of 0.7085–0.7089 and of –8.17 to –8.07 (T_{2DM} = 1.6 Ga), respectively. The Huangshitan granites display $(^{87}Sr/^{86}Sr)_i$ of 0.6844–0.7094 and $\varepsilon_{Nd}(t)$ values of –4.13 to –3.60 with T_{2DM} = 1.2 Ga. The wide-ranging $(^{87}Sr/^{86}Sr)_i$ of the Longyou, Shanghekou, and Huangshitan granitoids (especially for those <0.7) could be attributed to the high whole-rock Rb contents affected by post-magmatic processes and/or the low Sr contents caused by fractional crystallization of feldspar, which make it imprecise to measure the initial Sr isotopic compositions.

For those granitoids from the SE Zhejiang belt, they exhibit relatively uniform initial Sr isotopic composition for each pluton. The Xiaoxiong (quartz) syenitic porphyries, Zhujiajian granites, and Qingbang island granites have $(^{87}Sr/^{86}Sr)_i$ of 0.7075–0.7079, 0.7032–0.7034, and 0.6890–0.6955, respectively. For Nd isotopic composition, the Xiaoxiong (quartz) syenitic porphyries have restricted and relatively evolved Nd isotopic composition ($\varepsilon_{Nd}(t)$ = –3.67 to –3.42) with T_{2DM} = 1.2 Ga, while $\varepsilon_{Nd}(t)$ values of the Zhujiajian and Qingbang island granites range from –7.88 to –5.67, with T_{2DM} = 1.4–1.5 Ga.

5.4. Zircon Hf Isotope

The results for in situ zircon Hf isotopic analysis are listed in Supplementary Table DR3 and plotted in Figure 11.

For rocks from the NW Zhejiang belt, zircon $\varepsilon_{Hf}(t)$ values of the Sucun quartz monzonite SC05 (–10.92 to –7.83), Longyou granite LY03 (–12.75 to –7.45), and Shanghekou granite SHK07 (–15.07 to –10.62) are relatively intensive and low, while those of the Huangshitan granite HST03 (–45.58 to –2.16) are wide-ranged. However, the zircons with U-Pb ages close to magma crystallization age of the Huangshitan granite show relatively intensive $\varepsilon_{Hf}(t)$ values of –5.90 to –2.16, which could represent Hf isotopic composition of the magma. For rocks from the SE Zhejiang belt, ten analyses of zircons from the Xiaoxiong syenitic porphyry DSY81 yielded $\varepsilon_{Hf}(t)$ values of –5.76 to –2.25. In contrast, nine analyses of zircons from the Zhujiajian granite DSY92 and Qingbang island granite DJ18 give more evolved $\varepsilon_{Hf}(t)$ values of –10.60 to –6.32 and –8.25 to –5.67, respectively.

6. DISCUSSION

6.1. Classification of the Studied Granitoids

Among all the proposed classification schemes for granitoids, the I-S-M-A classification is widely accepted and utilized (Chappell and White, 1974; Whalen et al., 1987). A-type granite, therein, was firstly defined by Loiselle and Wones (1979) to describe the alkaline, anhydrous, and anorogenic features of the granitic rocks. They are high-temperature granites and geochemically characterized by high SiO_2, $Na_2O + K_2O$, REEs (except Eu), high field strength elements (e.g., Nb, Ta, Zr, and Hf) contents, and Ga/Al ratio and low CaO, Ba, Sr, and Eu contents (Collins et al., 1982; Whalen et al., 1987). For I-, S-, and M-type granites, they are

TABLE 2. DATA OF WHOLE-ROCK Sr AND Nd ISOTOPES FOR THE STUDIED GRANITOIDS FROM ZHEJIANG, NORTHEAST SOUTH CHINA BLOCK

Sample no.	Age (Ma)	$^{87}Rb/^{86}Sr$	$^{87}Sr/^{86}Sr$	2σ	$(^{87}Sr/^{86}Sr)_i$	$^{147}Sm/^{144}Nd$	$^{143}Nd/^{144}Nd$	2σ	$^{143}Nd/^{144}Nd(t)$	$\varepsilon_{Nd}(t)$	T_{DM} (Ga)	T_{2DM} (Ga)
Longyou granite												
LY01	132.4	11.1898	0.728841	0.000003	0.7078	0.1441	0.512183	0.000003	0.512058	–7.99	2.1	1.6
LY02	132.4	26.3982	0.752992	0.000003	0.7033	0.1582	0.512216	0.000005	0.512079	–7.58	2.6	1.5
LY03	132.4	22.0391	0.746058	0.000003	0.7046	0.1511	0.512204	0.000005	0.512073	–7.70	2.3	1.5
LY04	132.4	14.1016	0.734243	0.000004	0.7077	0.1295.	U.D.*	U.D.*	N.D.†	N.D.†	N.D.†	N.D.†
Shanghekou granite												
SHK03	131.3	125.7621	0.920219	0.000004	0.6855	0.1978	0.512246	0.000008	0.512076	–7.67	8.4	1.5
SHK05	131.3	51.4234	0.806211	0.000004	0.7102	0.1305	0.512167	0.000003	0.512055	–8.08	1.8	1.6
SHK06	131.3	232.6479	1.097610	0.000005	0.6634	0.2538	U.D.*	U.D.*	N.D.†	N.D.†	N.D.†	N.D.†
SHK07	131.3	73.7419	0.841297	0.000005	0.7037	0.1564	0.512191	0.000004	0.512056	–8.05	2.5	1.6
Sucun quartz monzonite												
SC01§	136.1	2.2049	U.D.*	U.D.*	N.D.†	0.1044	0.512140	0.000005	0.512047	–8.11	1.4	1.6
SC04§	136.1	2.2433	0.712875	0.000006	0.7085	0.1054	0.512138	0.000004	0.512044	–8.17	1.4	1.6
SC05§	136.1	2.3945	0.713086	0.000005	0.7085	0.1110	0.512148	0.000003	0.512049	–8.07	1.5	1.6
SC06§	136.1	2.1823	0.713080	0.000005	0.7089	0.1034	0.512141	0.000002	0.512049	–8.08	1.4	1.6
Huangshitan granite												
HST01	126.0	6.6219	0.721268	0.000006	0.7094	0.1229	0.512390	0.000007	0.512289	–3.65	1.3	1.2
HST02	126.0	84.0911	0.859306	0.000004	0.7087	0.1392	0.512406	0.000005	0.512291	–3.60	1.5	1.2
HST03	126.0	259.3056	1.148750	0.000004	0.6844	0.1777	0.512411	0.000008	0.512264	–4.13	3.1	1.2
Xiaoxiong (quartz) syenitic porphyry												
DSY75	100.3	4.0983	0.713547	0.000004	0.7077	0.1052	0.512390	0.000004	0.512321	–3.67	1.1	1.2
DSY77	100.3	3.2293	0.712461	0.000003	0.7079	0.0992	0.512389	0.000004	0.512324	–3.60	1.0	1.2
DSY80	100.3	7.4992	0.718171	0.000004	0.7075	0.0967	0.512397	0.000003	0.512334	–3.42	1.0	1.2
DSY81	100.3	4.0890	0.713588	0.000003	0.7078	0.0970	0.512386	0.000003	0.512323	–3.63	1.0	1.2
Zhujiajian granite												
DSY92	108.0	28.7368	0.747503	0.000003	0.7034	0.0985	0.512218	0.000004	0.512149	–6.83	1.2	1.5
DSY93	108.0	27.3432	0.745182	0.000004	0.7032	0.0958	0.512276	0.000006	0.512208	–5.67	1.1	1.4
Qingbang island granite												
DJ8	108.3	72.4260	0.803299	0.000006	0.6918	0.1667	0.512213	0.000005	0.512095	–7.88	3.0	1.5
DJ18	108.3	85.9665	0.821263	0.000005	0.6890	0.1451	0.512304	0.000003	0.512201	–5.80	1.9	1.4
DJ19	108.3	53.9280	0.778480	0.000003	0.6955	0.1699	0.512311	0.000004	0.512190	–6.02	2.9	1.4

Notes: $^{87}Rb/^{86}Sr$ and $^{147}Sm/^{144}Nd$ ratios are calculated using Rb, Sr, Sm, and Nd contents (Table 1), measured by inductively coupled plasma–mass spectrometry; $\varepsilon_{Nd}(t)$ values are calculated using present-day $(^{147}Sm/^{144}Nd)_{CHUR}$ = 0.1967 and $(^{143}Nd/^{144}Nd)_{CHUR}$ = 0.512638, CHUR—chondritic uniform reservoir; T_{DM} values are calculated using present-day $(^{147}Sm/^{144}Nd)_{DM}$ = 0.2137 and $(^{143}Nd/^{144}Nd)_{DM}$ = 0.51315; T_{2DM} is the two-stage Nd depleted mantle model age calculated using the same assumption formulation as Keto and Jacobsen (1987).

U.D.*—undetected.

N.D.†—no data.

§Data from Pan et al. (2018).

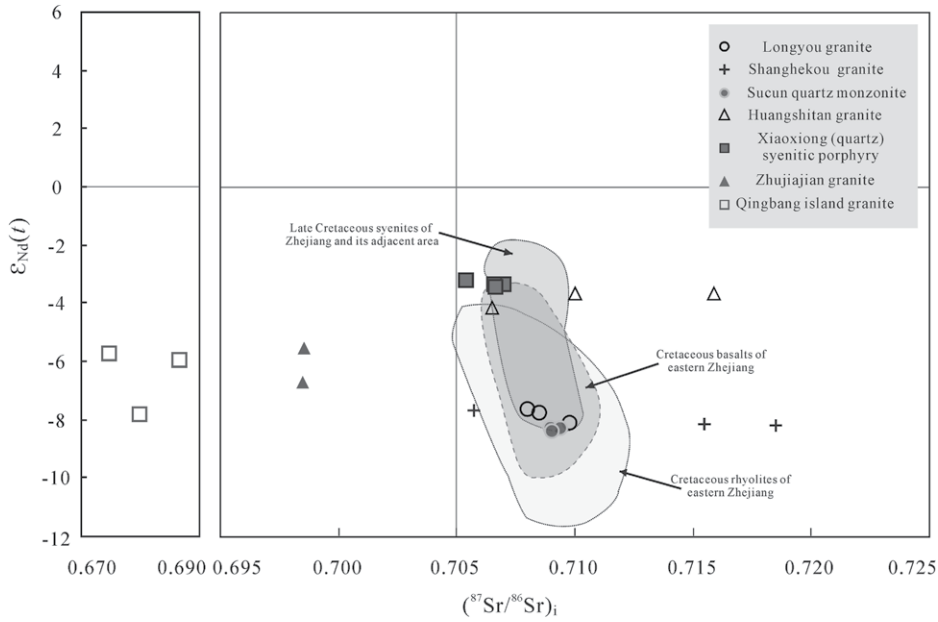

Figure 10. $\varepsilon_{Nd}(t)$ versus $(^{87}Sr/^{86}Sr)_i$ diagram for the studied granitoids and coeval basalts, rhyolites, and syenites from Zhejiang, northeast South China Block. The Cretaceous basalts and rhyolites of eastern Zhejiang from Yu et al. (1993), Chen and Zhou (1999), Shen et al. (1999), and Yang et al. (1999) and references therein. The Late Cretaceous syenites of Zhejiang and its adjacent area from Li and Jiang (2014) and He and Xu (2012) and references therein.

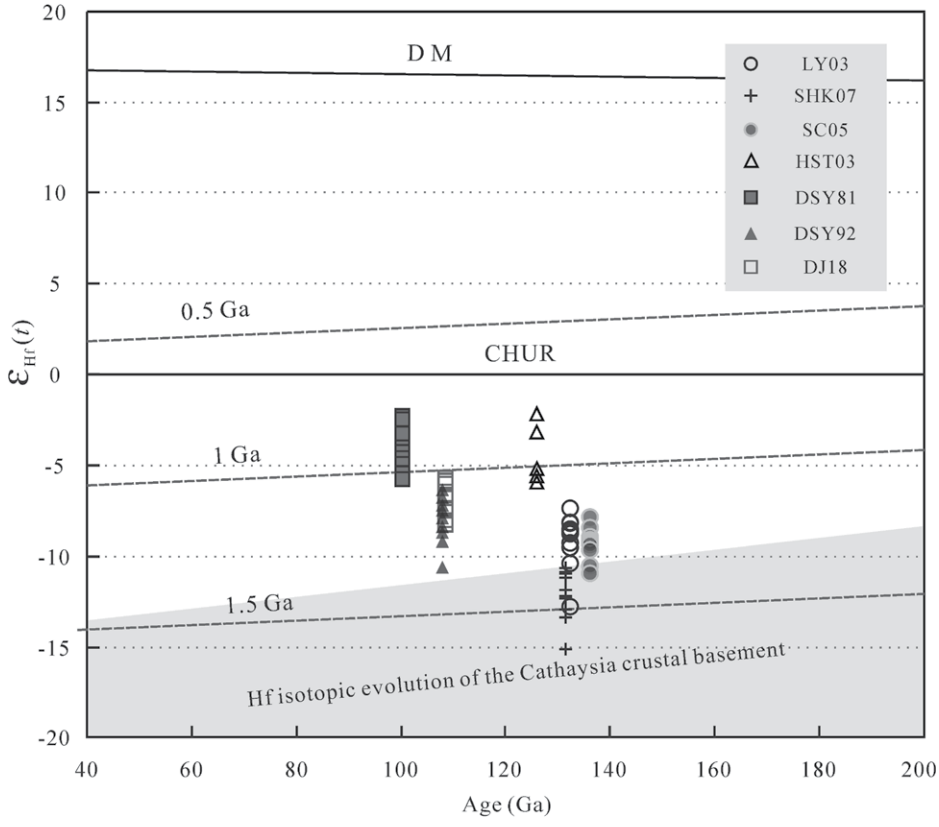

Figure 11. Plots of $\varepsilon_{Hf}(t)$ versus U-Pb ages for the studied granitoids from Zhejiang, northeast South China Block. Hf isotopic evolution for the Cathaysia crustal basement from Xu et al. (2007) and He and Xu (2012). CHUR—chondritic uniform reservoir; DM—depleted mantle.

classified by their different source rock compositions. M-type granite was suggested to be derived from subducted oceanic crust or overlying mantle (Pitcher, 1983; Whalen, 1985), while I- and S-type granites are derived from partial melting of meta-igneous source rocks and meta-sedimentary source materials, respectively (Chappell and White, 1974). Mineralogically, hornblende, and sphene are common in I-type granite, while aluminosilicates such as garnet, cordierite, and muscovite can be generally observed in S-type granite (Chappell and White, 1974, 2001). Geochemically, I-type granite displays higher Na_2O content than those of S-type granite at comparable SiO_2 content. Comparing with the relatively restricted high SiO_2 content of S-type granite, I-type granite holds a broader spectrum of composition. Additionally, I-type granite is mainly metaluminous, whereas S-type granite is strongly peraluminous (Chappell and White, 1974).

The pronouncedly evolved Sr-Nd-Hf isotopic compositions of the Longyou, Shanghekou, Sucun, Huangshitan, Zhujiajian, and Qingbang island granitoids absolutely rule out the possibility of mantle-derived magma (i.e., M-type granite) for their generation. Among the studied granitoids, samples from the Shanghekou, Huangshitan, Longyou, and Qingbang island plutons display affinity with A-type granite by their remarkable Ba, Sr, and Eu depletion and low Al_2O_3 and CaO contents (Table 1; Fig. 9). However, in all the Nb versus 10000*Ga/Al (Fig. 12), $K_2O + Na_2O$ versus 10000*Ga/Al, $(Na_2O + K_2O)/CaO$ versus Zr + Nb + Ce + Y, and TFeO/MgO versus Zr + Nb + Ce + Y discrimination diagrams (Supplementary Figs. DR1A–DR1C), only the Huangshitan granites fall into the field of A-type granites, while the Longyou, Shanghekou, Sucun, Zhujiajian, and Qingbang island granitoids are ambiguous with their plots straddling at or near the boundary line. This, together with their lower REE and Ga contents, Ga/Al ratio, and Zr saturation temperature than the typical A-type granite in Zhejiang area (Table 1; Fig. 13), indicates that only the Huangshitan granite among them is A-type granite.

We further classify the Longyou, Shanghekou, Sucun, Huangshitan, Zhujiajian, and Qingbang island granitoids as I-type granites by the following evidences: (1) samples from these plutons have high Na_2O contents (3.24–4.27 wt%), which is within the scope of Na_2O content of I-type granite (>3.2 wt%) defined by Chappell and White (1974), (2) the Sucun quartz monzonites have relatively mafic compositions with SiO_2 content of 67.71–68.93 wt%, which contradicts with high SiO_2 content of the S-type granite Chappell and White (1974), (3) no S-type granite-distinctive mineral like garnet, cordier-

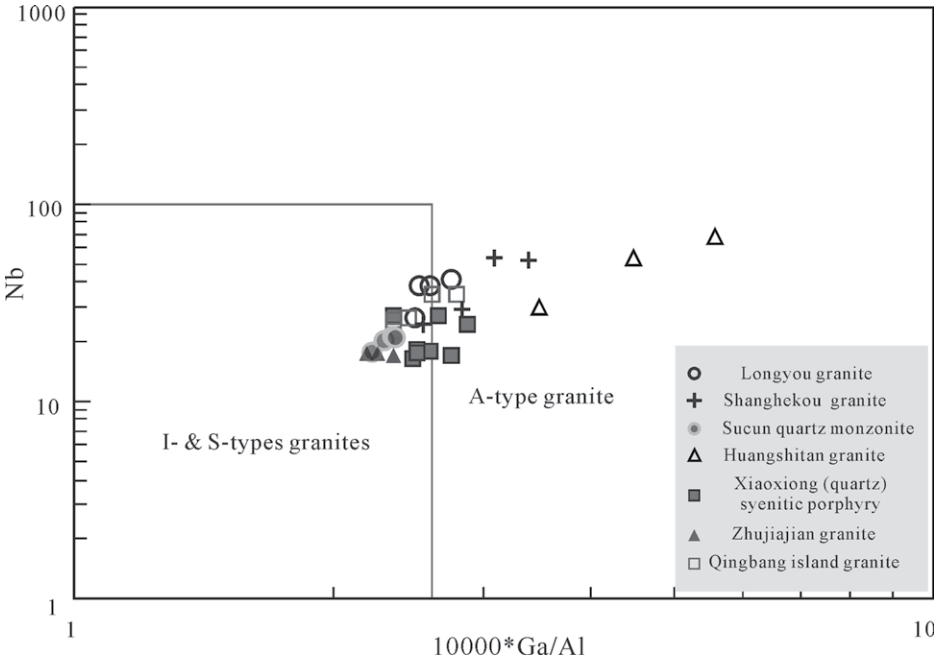

Figure 12. Nb versus 10000*Ga/Al discrimination diagram for the studied granitoids from Zhejiang, northeast South China Block (after Whalen et al., 1987). I-type granite—granite from partial melting of meta-igneous rocks; S-type granite—granite from partial melting of meta-sedimentary; A-type granite—granite with alkaline and anhydrous features from anorogenic setting.

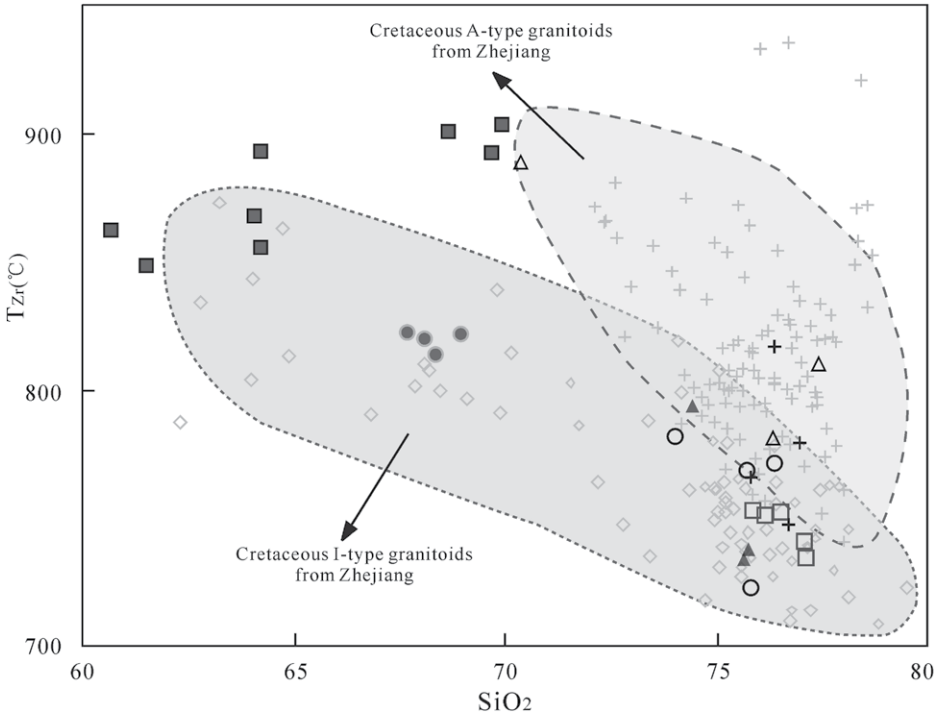

Figure 13. Plots of T_{Zr}(°C) versus SiO_2 for the Cretaceous granitoids from Zhejiang, northeast South China Block. Data sources of the granitoids are listed in Supplementary Table DR1. Symbols as those in Figure 12. T_{Zr}(°C)—Zr saturation temperature. See Figure 12 for definition of A- and I-types granites.

ite, and muscovite is observed in thin sections for all the samples, and (4) granitoids from the Longyou, Shanghekou, and Sucun plutons have I-type granite-like aluminum saturation index (ASI <1.1). It is worth noting that the Zhujiajian and Qingbang island granites are weakly-strongly peraluminous with relatively high ASI (1.07–1.13), which shows affinity with S-type granite. However, it is suggested by Chappell (1999) that ASI values of S- and I-type granites overlap with each other when the granites become highly evolved since Al-oversaturation is intrinsic to all of the most felsic granitic melts. At this condition, the I-S division by ASI is invalid for the highly fractionated Zhujiajian and Qingbang island granites.

The Xiaoxiong (quartz) syenitic porphyry is characterized by relatively depleted Nd-Hf isotopic and intermediate geochemical compositions. It differs from other studied granitoids by remarkably high alkali content and distinct trace elemental pattern, indicating a heterogenous magmatic source and/or different magmatic processes for their generation. We propose it could be a derivative of a mantle-derived melt when considering other research on coeval syenites in Zhejiang and its adjacent area (for details, see Section 6.2.2).

To sum up, the Huangshitan granite in the NW Zhejiang belt is an A-type granite and the Xiaoxiong (quartz) syenitic porphyry in the SE Zhejiang belt is a derivative of mantle-derived melts, while the Longyou, Shanghekou, and Sucun granites in the NW Zhejiang belt, together with the Qingbang island and Zhujiajian granites in the SE Zhejiang belt, are typical I-type granites.

6.2. Petrogenesis

6.2.1. The Longyou, Shanghekou, Sucun, Zhujiajian, and Qingbang Island I-type Granitoids

All the I-type granitoids in this study are characterized by high SiO_2, low MgO, Cr, and Ni contents, and pronouncedly evolved whole-rock Sr-Nd and zircon Hf isotopic compositions, which indicate the major role of old igneous crusts for their derivation. In addition, their Nd isotopic compositions and two-stage Nd model ages (1.4–1.6 Ga) are comparable with contemporary acidic rocks in Zhejiang (Fig. 10). It was suggested that intermediate-acidic igneous rocks contain too little water to yield large amounts of acidic magma except at high temperatures (Beard et al., 1993). Therefore, the intermediate-acidic igneous rocks as magmatic sources fail to account for the Cretaceous magmatic flare up in Zhejiang. By contrast, derivation of granitic magmas from low-degree partial melting of basaltic rocks is an effective way (Sisson et al., 2005). Geochemically, all the studied granitoids

have relatively intermediate K_2O and Na_2O contents and K_2O/Na_2O ratios. Therefore, they could not be melts extracted from amphibolite (Beard and Lofgren, 1991) or metabasalt (Rapp and Watson, 1995) that hold low K_2O and variable Na_2O content, but is similar to those from partial melting of medium- to high-K basaltic rock at mid-to-lower crustal levels (i.e., 20–25 km) (Sisson et al., 2005). For those melts extracted from K-rich basaltic rock, high Rb/Sr ratio is another feature besides their relatively high K_2O content. Although plagioclase fractionation during magmatic evolution is the overwhelming factor giving rise to the extremely high Rb/Sr ratio of the highly evolved granites from the Longyou, Shanghekou, Zhujiajian, and Qingbang island plutons, the granitoids with no obvious plagioclase fractionation from the Sucun pluton also display relatively high Rb/Sr ratios, which further confirm K-rich magmatic sources for their generation.

In addition to the significant role of crustal components for these granitoids, minor mantle-derived mafic magmas had also been incorporated. This deduction is supported by the following evidence: (1) $\varepsilon_{Hf}(t)$ values of zircons vary a lot for granitoids for the Sucun (–10.92 to –7.83), Longyou (–12.75 to –7.45), Shanghekou (–15.07 to –10.62), Zhujiajian (–10.60 to –6.32), and Qingbang island (–8.25 to –5.67) plutons, which is inconsistent with magma from a single source with Hf homogeneous isotopic composition. (2) Coupled with the Cretaceous granitoids in this study, large amounts of coeval mafic dykes/intrusions were emplaced in both the NW Zhejiang belt (Li et al., 2011; Qi et al., 2016; Pan et al., 2018) and the SE Zhejiang belt (Dong et al., 2010; Pan et al., 2014). Contemporaneous emplacement of granitoids and mafic rocks provide a good opportunity to cause the magma mixing, which is proved by the prevailing presence of MMEs in both the ca. 130 Ma granitoids in NW Zhejiang and the ca. 100 Ma granitoids in SE Zhejiang (Zhao et al., 2016). (3) A consensus has been reached that the mixing of crust- and mantle-derived magmas is a universal process for the generation of both the I-type granitoids in coastal Zhejiang (Xie et al., 2004; Zhang et al., 2005) and inland Zhejiang (Pan et al., 2018) and (4) as shown in the U-Pb zircon age versus $\varepsilon_{Hf}(t)$ diagram (Fig. 11), all the analyzed spots except for those from the Shanghekou granite are plotted at or above the evolution range of the Cathaysia crustal basement. Therefore, our studied I-type granitoids could be derived from partial melting of ancient K-rich crustal basaltic rocks with minor mafic magma incorporation.

As shown in Figure 8, elemental covariant relationships are observed for single pluton as well as among plutons. This, together with the remarkable Ba, Sr, P, Ti, and Eu depletion for the majority of the samples (Fig. 9), indicates that they had suffered from significant mineral fractional crystallization. The Longyou, Shanghekou, and Sucun granitoids were coevally emplaced in a restricted area and have genetic relationship with each other in the Harker diagrams (Fig. 8). Therefore, they are regarded as derivatives at different stages. Samples from the three plutons show gradually decreasing Al_2O_3 (Fig. 8D), CaO (Fig. 8G), Ba, Sr, and Eu (Table 1; Fig. 9A) with increasing SiO_2, which could result from fractionation of plagioclase. This is in agreement with the progressively decreasing volume of plagioclase in the Sucun (30%), Longyou (22–25%), and Shanghekou (18–20%) granitoids. The decreasing contents of MgO (Fig. 8B), TFeO (Fig. 8C), and TiO_2 (Fig. 8F) with increasing SiO_2 is likely caused by fractional crystallization of hornblende, Fe-Ti oxides, and titanite, which are present in the Sucun quartz monzonite (low SiO_2 contents) and relatively rare in the Longyou and Shanghekou granites (high SiO_2 contents). The decreasing P_2O_5 contents with increasing SiO_2 (Fig. 8E) in these three granites could be due to apatite fractionation. In chondrite-normalized REE patterns (Fig. 9B), the Sucun quartz monzonites exhibit higher light rare earth elements (LREE) and lower heavy rare earth elements (HREE) contents with more fractionated REE patterns $(La/Yb)_N$ ratios than the Longyou and Shanghekou granites. The drop in LREE contents could be related to the segregation of titanite and monazite. The increasing HREE, as well as Th and U contents, indicates that vast crystallization of zircon is a late-stage process during magma differentiation, which is consistent with the higher HREE, Th, and U contents in the zircons of the Longyou and Shanghekou granites than those of the Sucun quartz monzonite (not shown). In addition, above deduction is further supported by the higher whole-rock Zr contents in the Sucun quartz monzonites than those in the Longyou and Shanghekou granites (Table 1), as well as the appearance of zircon inclusions in biotite from the most highly evolved Shanghekou granite (Fig. 4D). For the geochemistry-homogeneous Zhujiajian and Qingbang island granites, they are supposed to have experienced similar magmatic differentiation because of their evolved compositions and depletion of Ba, Sr, P, Eu, and Ti.

In summary, these I-type granitoids generated by mixing of predominantly K-rich crustal basaltic rocks-derived melts and subordinately mantle-sourced mafic magma, with subsequent suffering from variable magmatic differentiation.

6.2.2. The Xiaoxiong (Quartz) Syenitic Porphyry

Compared to other granitoids, the Xiaoxiong (quartz) syenitic porphyries hold remarkably higher alkali content and are accordingly classified as alkaline series (Fig. 7A). For alkaline syenites, although volumetrically negligible, they have drawn much attention because of their specific petrogenesis and tectonic implications (e.g., Barker et al., 1975; Litvinovsky et al., 2002; Li et al., 2003). Three competitive opinions on their petrogenesis have been put forward, including: (1) they should be residual melt differentiating from an enriched mantle-derived basaltic magma with varying degrees of crustal assimilation (Litvinovsky et al., 2002; Li et al., 2003), (2) they are a mixture of mantle- and crustal-derived magmas (Mingram et al., 2000), and (3) they are derived from partial melting of thickened crustal rocks (Tchameni et al., 2001; Jiang et al., 2002). Isotopically, the Xiaoxiong (quartz) syenitic porphyries are more depleted in Nd isotopic compositions than those of the coeval crustal-derived rhyolites and the studied granitoids from eastern Zhejiang (Fig. 10). For Hf isotopic composition, they plot above the upper boundary line of the Hf evolutional region of the Cathaysia crustal basement (Fig. 11). Geochemically, comparing with other studied granitoids, they are more basic with SiO_2 of 60.68–69.92 wt% and display higher total REE contents and more fractionated REE patterns (Fig. 9D), which are also indicative of a different magmatic source for their generation. Moreover, available studies show that the Cathaysia Block is based by rock association of amphibolite, paragneiss, and schists (Shen et al., 1999; Xu et al., 2005). Among these lithologies, the paragneiss and schists host Eu/Eu* values lower than 0.76, and the schists are highly acidic with SiO_2 content >72 wt% (Zhang and Zhang, 1993). Hence, partial melting of these rocks at depth could not produce relatively low-SiO_2 melts without negative Eu anomaly like the Xiaoxiong (quartz) syenitic porphyries. The above lines of evidence absolutely exclude the major role of crustal materials as their magmatic source. As shown in the $\varepsilon_{Nd}(t)$ versus $(^{87}Sr/^{86}Sr)_i$ diagram (Fig. 10), the Xiaoxiong (quartz) syenitic porphyries are plotted at or near the most depleted area of field defined by contemporary basalts from eastern Zhejiang, which could not be attributed to mixture of enriched mantle- and crustal-derived magmas. This deduction is also supported by their restricted whole rock Sr-Nd and narrow-ranging zircon Hf isotopic compositions.

Therefore, the most likely mechanism to generate the Xiaoxiong pluton is fractional crystallization of basaltic magma from an enriched mantle source. It is worth noting that there are

some coeval enriched mantle-derived syenites reported at Zhejiang and its adjacent area, such as the Honggong, Yandangshan, Kangli, Fuzhou, Daheshan, and Zijinshan plutons (He and Xu, 2012; Li and Jiang, 2014 and references therein). The Xiaoxiong (quartz) syenitic porphyries display comparable Sr-Nd isotopic compositions (Fig. 10) and overlap in the trace element spider diagram (Fig. 9C) and chondrite-normalized REE pattern (Fig. 9D) with other studied syenites, indicating a homologous magma source for their generation. The observed depletion of Nb, Ta, and Ti for these syenites could be attributed to intrinsic features of their magma sources or their parental magma buffered by Ti-rich minerals as rutile and ilmenite. However, rutile or ilmenite fractional crystallization during magma evolvement or as residues during parting melting would not only give rise to the negative anomaly of Nb, Ta, and Ti, but also lead to depletion of Zr and Hf (Tiepolo et al., 2002; Klemme et al., 2005), which disaccords with the fact that no Zr or Hf anomaly of the Xiaoxiong (quartz) syenitic porphyries is observed. This, together with their enrichment of large-ion lithophile elements, suggests that the Xiaoxiong (quartz) syenitic porphyries probably sourced from enriched mantle metasomatized by slab-derived components. Considering the absence of Eu anomaly for the least evolved samples, the high K_2O signature of the Xiaoxiong pluton could be ascribed to a K-rich metasomatized mantle source with hydrous phases such as amphibole or phlogopite, like those reported by Conceição and Green (2004) and Conticelli et al. (2009).

The MgO, TFeO, P_2O_5, and TiO_2 decreasing with increasing SiO_2 contents for the Xiaoxiong (quartz) syenitic porphyry (Figs. 8B, 8C, 8E, and 8F) indicates extraction of hornblende/pyroxene, apatite, and Te-Ti oxides during magma evolution. The K_2O and Al_2O_3 contents firstly increase with SiO_2 increasing from 60 to 64 wt% and then decrease with SiO_2 increasing from 64 to 70 wt% (Figs. 8A and 8D), indicating that obvious fractional crystallization of feldspar did not occur until the magma was highly evolved (with SiO_2 content of ~64 wt%). This deduction is further supported by the phenomenon that only the samples with SiO_2 content higher than 64 wt% display obviously negative Eu anomalies (Table 1). Therefore, basaltic parental magma from K-rich metasomatized mantle followed by broad fractional crystallization is a feasible way to generate the Xiaoxiong pluton with high K_2O and SiO_2, low MgO, Cr, and Ni contents, and fractionated REE patterns.

6.2.3. The Huangshitan A-type Granite

For derivation of A-type granite, several petrogenetic models have been proposed: (1) partial melting of lower crustal granulitic residue from which a granitic melt was previously extracted (Collins et al., 1982; Clemens et al., 1986; Whalen et al., 1987), (2) direct fractionation products of mantle-derived melts (Eby, 1992; Turner et al., 1992; Han et al., 1997), (3) partial melting of calc-alkaline rocks (Creaser et al., 1991), and (4) hybridization between crustal-derived felsic and mantle-derived mafic magmas (Yang et al., 2006). The Huangshitan granite in this study possess negative zircon $\varepsilon_{Hf}(t)$ and $\varepsilon_{Nd}(t)$ values of –5.90 to –2.16 and –4.13 to –3.60, respectively, which differ a lot from those of contemporary mantle-derived mafic rocks nearby (Qi et al., 2016; Pan et al., 2018). Therefore, neither the juvenile crustal component nor the mantle material could be the major contributor for their generation. By contrast, the mature crustal materials could be the most feasible magmatic source, which is consistent with the previous investigations of A-type granites in a comparable area (Jiang et al., 2011; Yang et al., 2012; Li et al., 2013b; Sun et al., 2015).

In order to further constrain the source features of the Huangshitan granites, we compile the reported geochronological, geochemical, and Nd isotopic compositions of contemporary felsic magmatic rocks from the NW Zhejiang. The result reveals that the relatively low-temperature I-type granites are generally emplaced slightly earlier than the high-temperature A-type granites (Figs. 13 and 14A). Moreover, the later-emplaced granites generally display higher $\varepsilon_{Nd}(t)$ values than those of the former (Fig. 14B), which indicates more widespread incorporation of mantle-derived magma over time. The injected high-temperature mafic magma not only changed the isotopic composition of crustal magmatic sources, but also supplied sufficient heat to cause partial melting of the (refractory) ancient basement rocks that probably had been previously molten. Hence, the A-type Huangshitan granites were probably derived from partial melting of refractory ancient basement rocks with involvement of some high-temperature mafic magma during the peak period of the back-arc lithospheric extension in the NW Zhejiang belt (see Section 6.3). During the magmatic evolvement, the Huangshitan granite also suffered from widespread fractional crystallization of plagioclase, hornblende, apatite, and Te-Ti oxides. This conclusion is supported by the negative correlations between SiO_2 and Al_2O_3, CaO, MgO, TFeO, TiO_2, P_2O_5, Ba, Sr, and Eu (Figs. 8 and 9A).

6.3. Tectonic Implications

It is widely accepted that two major tectonic events successively affected the SCB during the Mesozoic (Chen et al., 2002; Zhou et al., 2006; Li and Li, 2007). In detail, collision of the Indochina Block with the SCB (i.e., the Indosinian Orogeny) around the southwest margin of the SCB dominated the early Mesozoic tectonic regime (Carter et al., 2001), while subduction of the Paleo-Pacific Plate beneath the SCB played a leading role in the late Mesozoic magmatism (Jahn, 1974; Huang and Zhao, 2006; Zhou et al., 2006). For the Mesozoic magmatism in Zhejiang, northeast SCB, it is noteworthy that igneous rocks did not develop until the eruption of the volcanic rocks named the Maonong Formation in the Early Jurassic (Liu et al., 2014). These volcanic rocks not only formed long after the collision of the Indochina Block and the SCB (ca. 250 Ma) in time scale (Carter et al., 2001), but also are far away from the suture zone in space. Therefore, they were unlikely generated at a post-collisional setting, but were highly possibly formed at the tectonic regime of subduction of the Paleo-Pacific Plate (Maruyama et al., 1997). The Early Jurassic Maonong Formation volcanics are only spatially restricted to the SE Zhejiang belt, which indicates that subduction of the Paleo-Pacific Plate toward the Zhejiang area had probably just started at that time and its influence was considered to be extremely weak (Jahn, 1974).

Different from the weak activity of the early Mesozoic magmatism, the late Mesozoic magmatism in the Zhejiang area is much stronger. As mentioned in Section 1, two magmatic pulses at ca. 145–120 Ma and ca. 110–85 Ma were figured out (Liu et al., 2012, 2014). The early episodic (ca. 145–120 Ma) magmatism in the SE Zhejiang belt is characterized by generation of large quantities of intermediate-acidic volcanics in the Moshishan Group (Figs. 1C and 2) (BGMRZP, 1989). They were suggested to be mainly derived from partial melting of ancient crustal materials (Liu et al., 2014). Such intense volcanism occurring within a short time indicates a sudden heat pulse. Underplating of the hot basaltic magma at the base of the continental crust could be the most potential heat source. This deduction is supported by the geophysical data (Liao et al., 1988) and petrological studies, which demonstrate existence of a high velocity-high density mafic layer under the coastal area of SE China (Xu et al., 1996, 1999). By consideration of their close relationship with the trench at that time, these mafic rocks could be derived from partial melting of the wet mantle wedge metasomatized by slab fluids. Therefore, we propose that the massive Early Cretaceous volcanics in the SE Zhejiang belt were generated at a continental arc setting.

Contemporaneous granitoids and their volcanic counterparts (i.e., the Jiande Group in Fig. 1C) in the NW Zhejiang belt are also

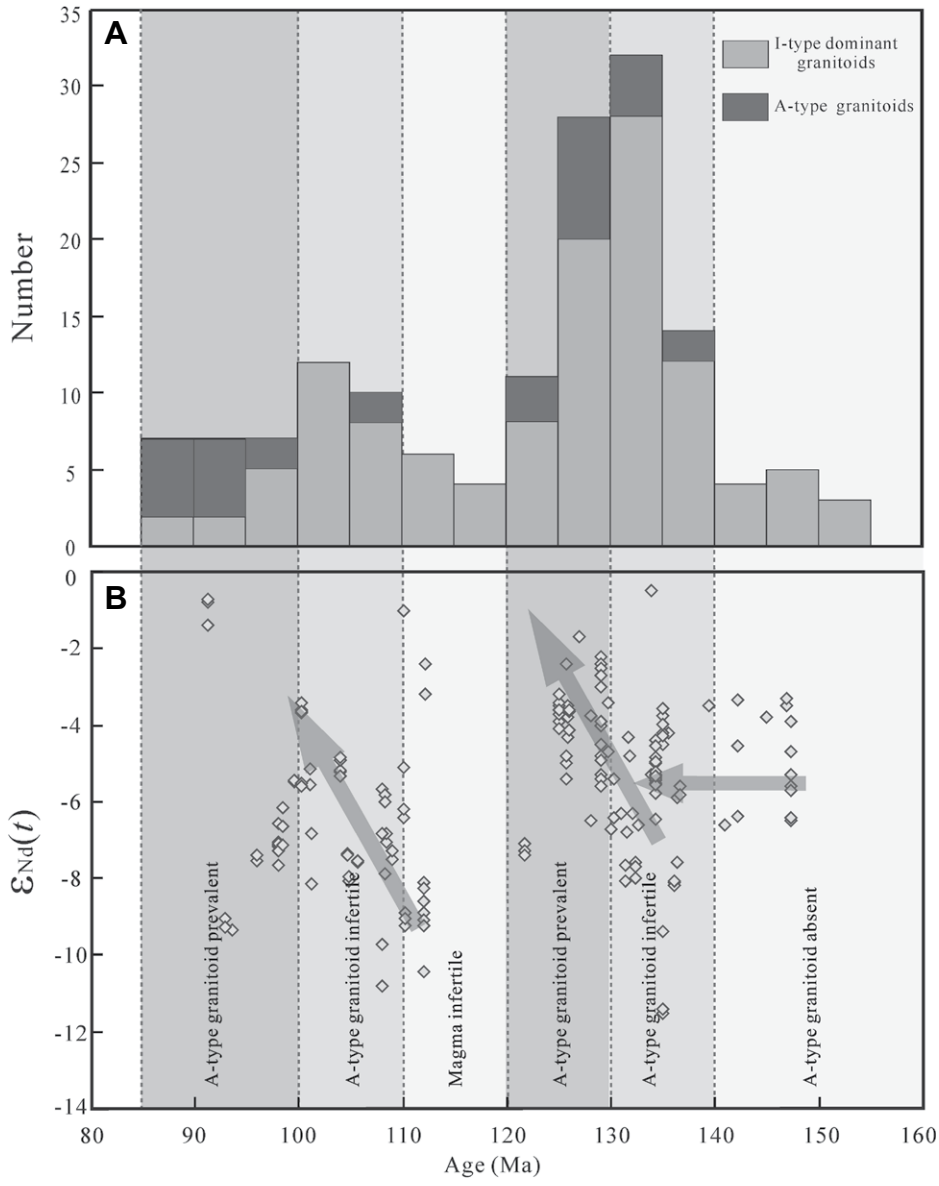

Figure 14. (A) Histogram showing age-spectrum of the Late Jurassic–Cretaceous granitoids in Zhejiang, northeast South China Block. (B) Plots of $\varepsilon_{Nd}(t)$ versus ages for the Late Jurassic–Cretaceous granitoids in Zhejiang, northeast South China Block. Data sources are listed in Supplementary Table DR1. See Figure 12 for definition of A- and I-types granites.

prevalent. These volcanics, deposited in the coeval large-scale NE-trending extensional basins (BGMRZP, 1989), indicate an extensional setting when they erupted. Coeval intrusions include both I-type and A-type granitoids. Available chronological data indicate that I-type granitoids spread throughout the period of the early episodic magmatism and reach climax ca. 140 Ma, whereas A-type granitoids share relatively narrow emplacement duration of 140–120 Ma and are not popular until 130 Ma (Fig. 14A). It is widely accepted that generation of A-type granites is related to an extensional setting (Martin et al., 1994; Bonin, 2007; Karsli et al., 2012). Therefore, coupled with generation of the volcanics in NE-trending extensional basins, emplacement of the A-type granites and flare-up of the I-type granites absolutely demonstrate an extensional setting. This opinion is further supported by emplacement of vast coeval NE- and NW-trending mafic dykes in the NW Zhejiang belt (BGMRZP, 1989). For this extensional tectono-magmatic event in the NW Zhejiang belt, two main competing tectonic models were put forward, including (1) a normal active continental arc following by slab roll-back of the Paleo-Pacific Plate (He and Xu, 2012; Li et al., 2013a, 2013b; Liu et al., 2014), and (2) back-arc extension induced by slab roll-back of the Paleo-Pacific Plate (Wong et al., 2009; Jiang et al., 2011). Considering that the Jurassic to Early Cretaceous granitoids are sparse (Li et al., 2013a, 2013b; Tang et al., 2014) and the limited Jurassic strata mainly consist of sedimentary rocks with few volcanic rocks in NW Zhejiang (BGMRZP, 1989), the NW Zhejiang belt is unlikely to be a continental magmatic arc at that time. In contrast, it was probably at a back-arc position since the SE Zhejiang belt is magmatically active and regarded as a continental arc. At this condition, initial back-arc extension might occur at ca. 140 Ma because of the prevalence of the I-type granitoids and coeval volcanics. Soon after, more extensive asthenospheric upwelling and back-arc lithospheric extension took place, which gave rise to the underplating of high-temperature mafic magmas and their accompanying crustal-derived melts. The mixture of these two magmatic endmembers generated both the A-type and I-type granitoids at ca. 135–120 Ma, which caused the progressively higher Nd isotopic composition (Fig. 14B).

For the late episodic (ca. 110–85 Ma) magmatism, the volcanic series named the Qujiang Group is poor in detrital contents and narrowly distributed in the NW Zhejiang belt (Figs. 1C and 2) (BGMRZP, 1989). By contrast, the coeval volcanism in the SE Zhejiang belt is much stronger (Figs. 1C and 2). Thus, comparing to the early episodic magmatism, the late episodic (ca. 110–85 Ma) magmatism shows obvious eastward migration, implying that the magmatic front progressively migrated eastward and the magmatism became inactive in interior Zhejiang. Meanwhile, coeval I- and A-type granites and dyke swarms are widespread in the NE Zhejiang belt, especially in the coastal area (Qiu et al., 2004; Dong et al., 2010; Chen et al., 2014a; Pan et al., 2014; Zhao et al., 2016), which indicates another extensional event occurred at that time. Along the coastal area, the I- and A-type granites are spatially symbiotic, exposed as composite granitic plutons such as the Putuoshan and Taohuadao plutons (Qiu et al., 2004). But overall, the I-type granitoids show relatively earlier magma crystallization ages (widespread from ca. 110 to 100 Ma) than those of the A-type granites (ca. 100–85 Ma) (Fig. 14A), which suggests that extensive extension probably took place at ca. 100 Ma. This deduction accords with the observations that T_{Zr} and Nd isotopic composition of the granitoids are progressively elevated over time (Figs. 13 and 14B). We propose that a new back-arc basin formed during this stage at the SE Zhejiang belt associated with the arc magmatism front back to the position of the East China Sea.

To sum up, two episodic back-arc extensions occurred in the Zhejiang area at ca. 140–120 Ma and ca. 110–85 Ma, respectively. Among the two extensional events, there exists a magmatic gap at ca. 120–110 Ma based on the available data (Fig. 14). Here we present a schematic tectonic model to describe the tectonic evolution of the Zhejiang area at the late Mesozoic (Fig. 15). The Zhejiang area experienced subduction of the Paleo-Pacific Plate as early as the Jurassic, which gave rise to continental arc magmatism at the SE Zhejiang belt. Subsequent slab roll-back initiated at ca. 140 Ma, causing upwelling of the hot asthenospheric materials to heat and melt the mantle wedge on the one hand and stretch the back-arc lithosphere on the other hand. Underplating of mantle wedge-derived mafic magmas at the base of the crust induced extensive magmatism at the magmatic front (represented by the Moshishan Group at the SE Zhejiang belt). Initial back-arc lithospheric extension at the NW Zhejiang belt resulted in a series of NE-trending basins and associated volcanics and coeval I-type granitoids (e.g., the Longyou, Sucun, and Shanghekou granitoids in this study) (Fig. 15A). Afterwards, intense back-arc lithospheric extension accompanying magmatic flare-up occurred since the fast slab roll-back at ca. 130–120 Ma (Fig. 15B). At this stage, both I-type and high-T A-type granitoids (e.g., the Huangshitan granite) are popular with more and more incorporated mantle-derived magma. Soon after, there came a stage of tectono-magmatic quiescence with eastward trench retreat at ca. 120–110 Ma, which was probably due to flat slab subduction (Fig. 15C). The magmatic front at this stage, accordingly, progressively migrated eastward at or even behind the current coastal area of the Zhejiang area. The second episodic slab roll-back initiated at ca. 110 Ma (Fig. 15D) and reached climax after ca. 100 Ma (Fig. 15E), generating the earlier I-type granitoids (e.g., Zhujiajian and Qingbang island granitoids) and later A-type granitoids and mantle-derived Xiaoxiong (quartz) syenitic porphyry at the SE Zhejiang belt (i.e., the site of back-arc extension at that time).

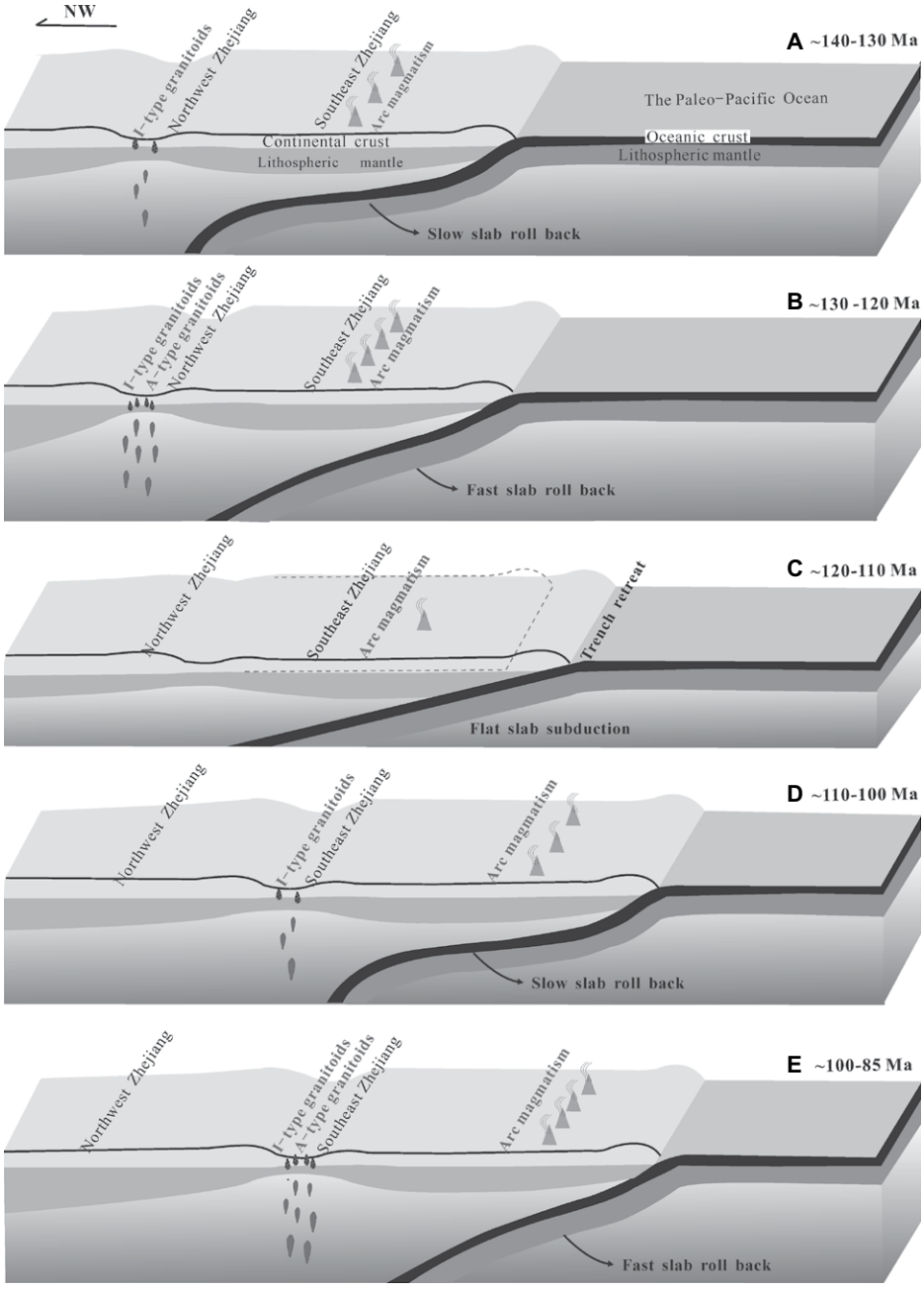

Figure 15. Schematic tectonic model for the late Mesozoic tectono-magmatic processes of the Paleo-Pacific Plate subduction system in Zhejiang area, northeast South China Block. See Figure 12 for definition of A- and I-types granites.

It is suggested that the East China Sea continental shelf, on the east of our study area (Fig. 1A), started rifting since the early Paleocene (e.g., Li et al., 2009a), which gave rise to formation of a series of NE-trending depressions. The same as the generation of the Mesozoic volcanic-sedimentary basins at Zhejiang, these NE-trending basins could also be related to episodic back-arc extension (Sibuet and Hsu, 1997) caused by downward bending of the Paleo-Pacific Plate (Zhou and Li, 2000). Coupled with the episodic back-arc extension and trench retreat at the inland and continental margin, subsequent episodic eastward retreat and roll-back of the Pacific Plate generated the West Philippine Basin, the Parece-Vela Basin, and the Mariana Trough at an oceanic setting. This episodic slab roll-back with trench retreat that generated earlier volcanic-sedimentary basins at a continental setting and later bark-arc basins at an oceanic setting provides an impressive style of oceanic slab subduction.

7. CONCLUSION

Seven granitic plutons from two Cretaceous granitic belts in the Zhejiang area, northeast South China Block, are studied to trace their petrogenesis and tectonic implications. The Sucun quartz monzonite, and the Longyou, Shanghekou, and Huangshitan granites from the NW Zhejiang belt show magma crystallization age of ca. 126–136 Ma, while the Xiaoxiong (quartz) syenitic porphyry, and the Zhujiajian and Qingbang island granites from the SE Zhejiang belt display younger magma crystallization age of ca.

100–108 Ma. Geochemical and isotopic studies on these granitoids indicate that the Sucun quartz monzonite, and Longyou, Shanghekou, Zhujiajian, and Qingbang island granites therein are fractionated I-type granites and were derived from ancient crustal melt-dominated magma with subsequent mineral fractional crystallization. The Huangshitan granite is supposed to be A-type granite from partial melting of mature crustal materials with some mantle-derived magma incorporation at a back-arc setting. In contrast, the alkaline Xiaoxiong (quartz) syenitic porphyry could be a derivative of basaltic magma from K-rich metasomatized mantle. With prior available studies, a two episodic slab roll-back model was put forward to account for generation of the studied granitoids: the older Longyou, Sucun, and Shanghekou I-type granitoids and the younger Huangshitan A-type granite from the NW Zhejiang belt, respectively, witnessed the initial and peak stages of the first episodic roll-back of the subducting Paleo-Pacific Plate from ca. 140 to 120 Ma, while the Zhujiajian and Qingbang island I-type granites and the Xiaoxiong (quartz) syenitic porphyry, together with the previously studied A-type granitoids (ca. 95–85 Ma) from the SE Zhejiang belt, recorded the initial and peak stages of the second episodic slab roll-back, respectively.

ACKNOWLEDGMENTS

This research is supported by the National Natural Science Foundation of China (grants: 41603026), the Fundamental Research Funds for the Central Universities, China University of Geosciences (Wuhan) (No. 2017053), and the Special Fund from the State Key Laboratory of Geological Processes and Mineral Resources, China University of Geosciences (Wuhan) (No. MSFGPMR14). We thank Dr. Hong-Fei Zhang for his helpful discussion and improving the paper. We would like to thank editors Brad Singer and Nick Timms and two anonymous reviewers for their constructive comments and suggestions that substantially improved our manuscript.

REFERENCES CITED

Barker, F., Wones, D.R., Sharp, W.N., and Desborough, G.A., 1975, The Pikes Peak batholith, Colorado front range, and a model for the origin of the gabbro-anorthosite-syenite-potassic granite suite: Precambrian Research, v. 2, p. 97–160, https://doi.org/10.1016/0301-9268(75)90001-7.

Beard, J.S., and Lofgren, G.E., 1991, Dehydration melting and water-saturated melting of basaltic and andesitic greenstones and amphibolites at 1, 3, and 6.9 kb: Journal of Petrology, v. 32, p. 365–401, https://doi.org/10.1093/petrology/32.2.365.

Beard, J.S., Abitz, R.J., and Lofgren, G.E., 1993, Experimental melting of crustal xenoliths from Kilbourne Hole, New Mexico and implications for the contamination and genesis of magmas: Contributions to Mineralogy and Petrology, v. 115, p. 88–102, https://doi.org/10.1007/BF00712981.

Blichert-Toft, J., and Albarede, F., 1997, The Lu-Hf isotope geochemistry of chondrites and the evolution of the mantle-crust system: Earth and Planetary Science Letters, v. 148, p. 243–258, https://doi.org/10.1016/S0012-821X(97)00040-X.

Bonin, B., 2007, A-type granites and related rocks: Evolution of a concept, problems and prospects: Lithos, v. 97, p. 1–29, https://doi.org/10.1016/j.lithos.2006.12.007.

Bureau of Geology and Mineral Resources of Zhejiang Province (BGMRZP), 1989, Regional Geology of Zhejiang Province [in Chinese]: Beijing, China, Geological Publishing House, 688 p.

Carlson, R.L., and Melia, P.J., 1984, Subduction hinge migration: Tectonophysics, v. 102, p. 399–411, https://doi.org/10.1016/0040-1951(84)90024-6.

Carter, A., Roques, D., Bristow, C., and Kinny, P., 2001, Understanding Mesozoic accretion in Southeast Asia: Significance of Triassic thermotectonism: Geology, v. 29, p. 211–214, https://doi.org/10.1130/0091-7613(2001)029<0211:UMAISA>2.0.CO;2.

Chappell, B.W., 1999, Aluminium saturation in I- and S-type granites and the characterization of fractionated haplogranites: Lithos, v. 46, p. 535–551, https://doi.org/10.1016/S0024-4937(98)00086-3.

Chappell, B.W., and White, A.J.R., 1974, Two contrasting granite types: Pacific Geology, v. 8, p. 173–174.

Chappell, B.W., and White, A.J.R., 2001, Two contrasting granite types: 25 years later: Journal of the Geological Society of Australia, v. 48, p. 489–499, https://doi.org/10.1046/j.1440-0952.2001.00882.x.

Charvet, J., 2013, The Neoproterozoic–Early Paleozoic tectonic evolution of the South China Block: An overview: Journal of Asian Earth Sciences, v. 74, p. 198–209, https://doi.org/10.1016/j.jseaes.2013.02.015.

Charvet, J., Lapierre, H., and Yu, Y., 1994, Geodynamic significance of the Mesozoic volcanism of southeastern China: Journal of Asian Earth Sciences, v. 9, p. 387–396, https://doi.org/10.1016/0743-9547(94)90050-7.

Chen, C., Lin, W., Lu, H., Lee, C., Tien, J., and Lai, Y., 2000, Cretaceous fractionated I-type granitoids and metaluminous A-type granites in SE China: the Late Yanshanian post-orogenic magmatism: Transactions of the Royal Society of Edinburgh. Earth Sciences, v. 91, p. 195–205, https://doi.org/10.1017/S0263593300007379.

Chen, C., Lee, C., and Shinjo, R., 2016, The epilog of the western paleo-Pacific subduction: Inferred from spatial and temporal variations and geochemistry of the Late Cretaceous to Early Cenozoic silicic magmatism in coastal South China: Journal of Asian Earth Sciences, v. 115, p. 520–546, https://doi.org/10.1016/j.jseaes.2015.10.002.

Chen, J.F., and Jahn, B.M., 1998, Crustal evolution of southeastern China: Nd and Sr isotopic evidence: Tectonophysics, v. 284, p. 101–133, https://doi.org/10.1016/S0040-1951(97)00186-8.

Chen, N., Dong, J., Chen, J., Dong, C., and Shen, Z., 2014a, Geometry and emplacement of the Late Cretaceous mafic dyke swarms on the islands in Zhejiang Province, Southeast China: Insights from high-resolution satellite images: Journal of Asian Earth Sciences, v. 79, p. 302–311, https://doi.org/10.1016/j.jseaes.2013.10.001.

Chen, P., Hua, R., Zhang, B., Lu, J., and Fan, C., 2002, Early Yanshanian post-orogenic granitoids in the Nanling region: Science in China. Series D, Earth Sciences, v. 45, p. 755–768, https://doi.org/10.1007/bf02878432.

Chen R. and Zhou J. C., 1999, Information of crust-mantle interaction implied in Early Cretaceous composite lavas and dikes from eastern Zhejiang [in Chinese with English abstract]: Geology Review, v. 45, p. 784–795, https://doi.org/10.16509/j.georeview.1999.s1.102.

Chen Y., Wang D., Xu Z. and Huang F., 2014b, Outline of regional metallogeny of ore deposits associated with the Mesozoic magmatism in South China [in Chinese with English abstract]: Geotectonica Et Metallogenia, v. 38, p. 219–229, https://doi.org/10.16539/j.ddgzyckx.2014.02.002.

Clemens, J.D., Holloway, J.R., and White, A.J.R., 1986, Origin of an A-type granite: Experimental constraints: The American Mineralogist, v. 71, p. 317–324.

Collins, W.J., Beams, S.D., White, A.J.R., and Chappell, B.W., 1982, Nature and origin of A-type granites with particular reference to SE Australia: Contributions to Mineralogy and Petrology, v. 80, p. 189–200, https://doi.org/10.1007/BF00374895.

Conceição, O.R.V., and Green, D.H., 2004, Derivation of potassic (shoshonitic) magmas by decompression melting of phlogopite + pargasite lherzolite: Lithos, v. 72, p. 209–229, https://doi.org/10.1016/j.lithos.2003.09.003.

Conticelli, S., Guarnieri, L., Farinelli, A., Mattei, M., Avanzinelli, R., Bianchini, G., Boari, E., Tommasini, S., Tiepolo, M., and Prelevi, D., 2009, Trace elements and Sr-Nd-Pb isotopes of K-rich, shoshonitic, and calc-alkaline magmatism of the Western Mediterranean Region: Genesis of ultrapotassic to calc-alkaline magmatic associations in a post-collisional geodynamic setting: Lithos, v. 107, p. 68–92, https://doi.org/10.1016/j.lithos.2008.07.016.

Creaser, R.A., Price, R.C., and Wormald, R.J., 1991, A-type granites revisited: Assessment of a residual-source model: Geology, v. 19, p. 163, https://doi.org/10.1130/0091-7613(1991)019<0163:ATGRAO>2.3.CO;2.

Deschamps, A., and Lallemand, S., 2002, The West Philippine Basin: An Eocene to early Oligocene back arc basin opened between two opposed subduction zones: Journal of Geophysical Research. Solid Earth, v. 107, p. 1–24, https://doi.org/10.1029/2001JB001706.

Dong, C.W., Yan, Q., and Zhang, D.R., 2010, Late Mesozoic extension in the coastal area of Zhejiang and Fujian provinces: A petrologic indicator from the Dongji Island mafic dike swarms [in Chinese with English abstract]: Yanshi Xuebao, v. 26, p. 1195–1203.

Dong, S.W., Zhang, Y.Q., Gao, R., Su, J.B., Liu, M., and Li, J.H., 2015, A possible buried Paleoproterozoic collisional orogen beneath central South China: Evidence from seismic-reflection profiling: Precambrian Research, v. 264, p. 1–10, https://doi.org/10.1016/j.precamres.2015.04.003.

Eby, G.N., 1992, Chemical subdivision of the A-type granitoids: Petrogenetic and tectonic implications: Geology, v. 20, p. 641, https://doi.org/10.1130/0091-7613(1992)020<0641:CSOTAT>2.3.CO;2.

Ernst, W.G., Tsujimori, T., Zhang, R., and Liou, J.G., 2007, Permo-Triassic collision, subduction-zone metamorphism, and tectonic exhumation along the east Asian continental margin: Annual Review of Earth and Planetary Sciences, v. 35, p. 73–110, https://doi.org/10.1146/annurev.earth.35.031306.140146.

Fryer, P., 1996, Evolution of the Mariana convergent plate margin system: Reviews of Geophysics, v. 34, p. 89–125, https://doi.org/10.1029/95RG03476.

Gao, S., Ling, W., Qiu, Y., Lian, Z., and Simon, K., 1999, Contrasting geochemical and Sm-Nd isotopic compositions of Archean metasediments from the Kongling high-grade terrain of the Yangtze craton: Evidence for cratonic evolution and redistribution of REE during crustal anatexis: Geochimica et Cosmochimica Acta, v. 63, p. 2071–2088, https://doi.org/10.1016/S0016-7037(99)00153-2.

Gao, S., Rudnick, R.L., Yuan, H.L., Liu, X.M., Liu, Y.S., Xu, W.L., Ling, W.L., Ayers, J., Wang, X.C., and Wang, Q.H., 2004, Recycling lower continental crust in the North China craton: Nature, v. 432, p. 892–897, https://doi.org/10.1038/nature03162.

Guo, J.L., Wu, Y.B., Gao, S., Jin, Z.M., Zong, K.Q., Hu, Z.C., Chen, K., Chen, H.H., and Liu, Y.S., 2015, Episodic Paleoarchean–Paleoproterozoic (3.3–2.0 Ga) granitoid magmatism in Yangtze Craton, South China: Implications for late Archean tectonics: Precambrian Research, v. 270, p. 246–266, https://doi.org/10.1016/j.precamres.2015.09.007.

Han, B., Wang, S., Jahn, B., Hong, D., Kagami, H., and Sun, Y., 1997, Depleted-mantle source for the Ulungur River A-type granites from North Xinjiang, China: Geochemistry and Nd-Sr isotopic evidence, and implications for Phanerozoic crustal growth: Chemical Geology, v. 138, p. 135–159, https://doi.org/10.1016/S0009-2541(97)00003-X.

He, C., Xu, C., Zhao, Z., Kynicky, J., Song, W., and Wang, L., 2017, Petrogenesis and mineralization of REE-rich granites in Qingxi and Guanxi, Nanling region, South China: Ore Geology Reviews, v. 81, p. 309–325, https://doi.org/10.1016/j.oregeorev.2016.10.021.

He, Z.Y., and Xu, X., 2012, Petrogenesis of the late Yanshanian mantle-derived intrusions in southeastern China: Response to the geodynamics of paleo-Pacific plate

subduction: Chemical Geology, v. 328, p. 208–221, https://doi.org/10.1016/j.chemgeo.2011.09.014.

Hu, X., Xu, J., Tong, C., and Chen, C., 1991, The Precambrian Geology of Southwestern Zhejiang Province [in Chinese]: Beijing, China, Geological Publishing House, 278 p.

Hu, Z., Liu, Y., Gao, S., Liu, W., Zhang, W., Tong, X., Lin, L., Zong, K., Li, M., Chen, H., Zhou, L., and Yang, L., 2012, Improved in situ Hf isotope ratio analysis of zircon using newly designed X skimmer cone and jet sample cone in combination with the addition of nitrogen by laser ablation multiple collector ICP-MS: Journal of Analytical Atomic Spectrometry, v. 27, p. 1391–1399, https://doi.org/10.1039/c2ja30078 h.

Huang, J., and Zhao, D., 2006, High-resolution mantle tomography of China and surrounding regions: Journal of Geophysical Research. Solid Earth, v. 111, no. B9, https://doi.org/10.1029/2005JB004066.

Jackson, S.E., Pearson, N.J., Griffin, W.L., and Belousova, E.A., 2004, The application of laser ablation-inductively coupled plasma-mass spectrometry to in situ U-Pb zircon geochronology: Chemical Geology, v. 211, p. 47–69, https://doi.org/10.1016/j.chemgeo.2004.06.017.

Jahn, B.M., 1974, Mesozoic thermal events in Southeast China: Nature, v. 248, p. 480–483, https://doi.org/10.1038/248480a0.

Jahn, B., Chen, P.Y., and Yen, T.P., 1976, Rb-Sr ages of granitic rocks in southeastern China and their tectonic significance: Geological Society of America Bulletin, v. 87, p. 763–776, https://doi.org/10.1130/0016-7606(1976)87<763:RAOGRI>2.0.CO;2.

Jiang, Y.H., Jiang, S., Ling, H., Zhou, X., Rui, X., and Yang, W., 2002, Petrology and geochemistry of shoshonitic plutons from the western Kunlun orogenic belt, Xinjiang, northwestern China: Implications for granitoid geneses: Lithos, v. 63, p. 165–187, https://doi.org/10.1016/S0024-4937(02)00140-8.

Jiang, Y.H., Zhao, P., Zhou, Q., Liao, S., and Jin, G., 2011, Petrogenesis and tectonic implications of Early Cretaceous S- and A-type granites in the northwest of the Gan-Hang rift, SE China: Lithos, v. 121, p. 55–73, https://doi.org/10.1016/j.lithos.2010.10.001.

Jiang, Y., Wang, G., Liu, Z., Ni, C., Qing, L., and Zhang, Q., 2015, Repeated slab advance-retreat of the Palaeo-Pacific plate underneath SE China: International Geology Review, v. 57, p. 472–491, https://doi.org/10.1080/00206814.2015.1017775.

Karsli, O., Caran, E., Dokuz, A., Oban, H., Chen, B., and Kandemir, R., 2012, A-type granitoids from the Eastern Pontides, NE Turkey: Records for generation of hybrid A-type rocks in a subduction-related environment: Tectonophysics, v. 530–531, p. 208–224, https://doi.org/10.1016/j.tecto.2011.12.030.

Keto, L.S., and Jacobsen, S.B., 1987, Nd and Sr isotopic variations of Early Paleozoic oceans: Earth and Planetary Science Letters, v. 84, p. 27–41, https://doi.org/10.1016/0012-821X(87)90173-7.

Klemme, S., Prowatke, S., Hametner, K., and Günther, D., 2005, Partitioning of trace elements between rutile and silicate melts: Implications for subduction zones: Geochimica et Cosmochimica Acta, v. 69, p. 2361–2371, https://doi.org/10.1016/j.gca.2004.11.015.

Lapierre, H., Jahn, B.M., Charvet, J., and Yu, Y.W., 1997, Mesozoic felsic arc magmatism and continental olivine tholeiites in Zhejiang Province and their relationship with the tectonic activity in southeastern China: Tectonophysics, v. 274, p. 321–338, https://doi.org/10.1016/S0040-1951(97)00009-7.

Li, B., and Jiang, S., 2014, Geochronology and geochemistry of Cretaceous Nanshanping alkaline rocks from the Zijinshan district in Fujian Province, South China: Implications for crust-mantle interaction and lithospheric extension: Journal of Asian Earth Sciences, v. 93, p. 253–274, https://doi.org/10.1016/j.jseaes.2014.07.040.

Li, C.F., Zhou, Z., Ge, H., and Mao, Y., 2009a, Rifting process of the Xihu Depression, East China Sea Basin: Tectonophysics, v. 472, p. 135–147, https://doi.org/10.1016/j.tecto.2008.04.026.

Li F., Zhou H., Tang Z., Li Y., Wang F., Xu Y., Qin H., Luo W. and Guan C., 2011, U-Pb ages, geochemistry and tectonic implications of mafic dyke swarms in Mugua, Chun'an county, Zhejiang Province [in Chinese with English abstract]: Geochimica, v. 40, p. 22–34, https://doi.org/10.19700/j.0379-1726.2011.01.003.

Li, H., Ling, M., Li, C., Zhang, H., Ding, X., Yang, X., Fan, W., Li, Y., and Sun, W., 2012, A-type granite belts of two chemical subgroups in central eastern China: Indication of ridge subduction: Lithos, v. 150, p. 26–36, https://doi.org/10.1016/j.lithos.2011.09.021.

Li, J., Ma, Z., Zhang, Y., Dong, S., Li, Y., Lu, M.A., and Tan, J., 2014, Tectonic evolution of Cretaceous extensional basins in Zhejiang Province, eastern South China: Structural and geochronological constraints: International Geology Review, v. 56, p. 1602–1629, https://doi.org/10.1080/00206814.2014.951978.

Li, P., Yu, X., Li, H., Qiu, J., and Zhou, X., 2013a, Jurassic–Cretaceous tectonic evolution of Southeast China: Geochronological and geochemical constraints of Yanshanian granitoids: International Geology Review, v. 55, p. 1202–1219, https://doi.org/10.1080/00206814.2013.771952.

Li, W.X., Li, X., Li, Z., and Lou, F., 2008, Obduction-type granites within the NE Jiangxi Ophiolite: Implications for the final amalgamation between the Yangtze and Cathaysia Blocks: Gondwana Research, v. 13, p. 288–301, https://doi.org/10.1016/j.gr.2007.12.010.

Li, X.H., Sun, M., Wei, G.J., Liu, Y., Lee, C.Y., and Malpas, J., 2000, Geochemical and Sm-Nd isotopic study of amphibolites in the Cathaysia Block, southeastern China: Evidence for an extremely depleted mantle in the Paleoproterozoic: Precambrian Research, v. 102, p. 251–262, https://doi.org/10.1016/S0301-9268(00)00067-X.

Li, X.H., Chen, Z., Liu, D., and Li, W., 2003, Jurassic gabbro-granite-syenite suites from southern Jiangxi Province, SE China: Age, origin, and tectonic significance: International Geology Review, v. 45, p. 898–921, https://doi.org/10.2747/0020-6814.45.10.898.

Li, X.H., Li, W., Li, Z., Lo, C., Wang, J., Ye, M., and Yang, Y., 2009b, Amalgamation between the Yangtze and Cathaysia Blocks in South China: Constraints from SHRIMP U-Pb zircon ages, geochemistry and Nd-Hf isotopes of the Shuangxiwu volcanic rocks: Precambrian Research, v. 174, p. 117–128, https://doi.org/10.1016/j.precamres.2009.07.004.

Li, Z., and Li, X., 2007, Formation of the 1300-km-wide intracontinental orogen and postorogenic magmatic province in Mesozoic South China: A flat-slab subduction model: Geology, v. 35, p. 179–182, https://doi.org/10.1130/G23193A.1.

Li, Z.X., Li, X.H., Wartho, J.A., Clark, C., Li, W.X., Zhang, C.L.L., and Bao, C., 2010, Magmatic and metamorphic events during the early Paleozoic Wuyi-Yunkai orogeny, southeastern South China: New age constraints and pressure-temperature conditions: Geological Society of America Bulletin, v. 122, p. 772–793, https://doi.org/10.1130/B30021.1.

Li, Z., Zhou, J., Mao, J., Santosh, M., Yu, M., Li, Y., Hu, Y., Langmuir, C.H., Chen, Z., and Cai, X., 2013b, Zircon U-Pb geochronology and geochemistry of two episodes of granitoids from the northwestern Zhejiang Province, SE China: Implication for magmatic evolution and tectonic transition: Lithos, v. 179, p. 334–352, https://doi.org/10.1016/j.lithos.2013.07.014.

Liao, Q.L., Wang, Z.M., Wang, P.L., Yu, Z.K., and Liu, B.C., 1988, Explosion seismic study of the crustal structure in Fuzhou-Quanzhou-Shantou region [in Chinese with English abstract]: Chinese Journal of Geophysics, v. 31, p. 270–280.

Litvinovsky, B.A., Jahn, B.M., Zanvilevich, A.N., Saunders, A., and Titov, A.V., 2002, Petrogenesis of syenite-granite suites from the Bryansky Complex (Transbaikalia, Russia): Implications for the origin of A-type granitoid magmas: Chemical Geology, v. 189, p. 105–133, https://doi.org/10.1016/S0009-2541(02)00142-0.

Liu, L., Xu, X., and Zou, H., 2012, Episodic eruptions of the Late Mesozoic volcanic sequences in southeastern Zhejiang, SE China: Petrogenesis and implications for the geodynamics of paleo-Pacific subduction: Lithos, v. 154, p. 166–180, https://doi.org/10.1016/j.lithos.2012.07.002.

Liu, L., Xu, X., and Xia, Y., 2014, Cretaceous Pacific plate movement beneath SE China: Evidence from episodic volcanism and related intrusions: Tectonophysics, v. 614, p. 170–184, https://doi.org/10.1016/j.tecto.2013.12.007.

Liu, L., Qiu, J., and Zhao, J., 2016, A hybrid origin for two Cretaceous monzonitic plutons in eastern Zhejiang Province, Southeast China: Geochronological, geochemical, and Sr-Nd-Hf isotopic evidence: Journal of Asian Earth Sciences, v. 115, p. 183–203, https://doi.org/10.1016/j.jseaes.2015.09.022.

Liu, Y., Zong, K., Kelemen, P.B., and Gao, S., 2008, Geochemistry and magmatic history of eclogites and ultramafic rocks from the Chinese continental scientific drill hole: Subduction and ultrahigh-pressure metamorphism of lower crustal cumulates: Chemical Geology, v. 247, p. 133–153, https://doi.org/10.1016/j.chemgeo.2007.10.016.

Liu, Y., Gao, S., Hu, Z., Gao, C., Zong, K., and Wang, D., 2010, Continental and oceanic crust recycling-induced melt-peridotite interactions in the Trans-North China Orogen: U-Pb dating, Hf isotopes and trace elements in zircons from mantle xenoliths: Journal of Petrology, v. 51, p. 537–571, https://doi.org/10.1093/petrology/egp082.

Loiselle, M.C., and Wones, D.R., 1979, Characteristics and origin of anorogenic granites: Geological Society of America Abstracts with Programs, v. 11, p. 468.

Maniar, P.D., and Piccoli, P.M., 1989, Tectonic discrimination of granitoids: Geological Society of America Bulletin, v. 101, p. 635–643, https://doi.org/10.1130/0016-7606(1989)101<0635:TDOG>2.3.CO;2.

Martin, H., Bonin, B., Capdevila, R., Jahn, B.M., Lameyre, J., and Wang, Y., 1994, The Kuiqi peralkaline granitic complex (SE China): Petrology and geochemistry: Journal of Petrology, v. 35, p. 983–1015, https://doi.org/10.1093/petrology/35.4.983.

Maruyama, S., Isozaki, Y., Kimura, G., and Terabayashi, M., 1997, Paleogeographic maps of the Japanese Islands: Plate tectonic synthesis from 750 Ma to the present: The Island Arc, v. 6, p. 121–142, https://doi.org/10.1111/j.1440-1738.1997.tb00043.x.

Middlemost, E.A.K., 1994, Naming materials in the magma/igneous rock system: Annual Review of Earth and Planetary Sciences, v. 37, p. 215–224, https://doi.org/10.1016/0012-8252(94)90029-9.

Miller, C.F., McDowell, S.M., and Mapes, R., 2003, Hot and cold granites? Implications of zircon saturation temperatures and preservation of inheritance: Geology, v. 31, no. 6, p. 529–532, https://doi.org/10.1130/0091-7613(2003)031<0529:HACGIO>2.0.CO;2.

Mingram, B., Trumbull, R.B., Littman, S., and Gerstenberger, H., 2000, A petrogenetic study of anorogenic felsic magmatism in the Cretaceous Paresis ring complex, Namibia: Evidence for mixing of crust and mantle-derived components: Lithos, v. 54, p. 1–22, https://doi.org/10.1016/S0024-4937(00)00033-5.

Nakakuki, T., and Mura, E., 2013, Dynamics of slab rollback and induced back-arc basin formation: Earth and Planetary Science Letters, v. 361, p. 287–297, https://doi.org/10.1016/j.epsl.2012.10.031.

Pan, F., Jin, C., Jia, B., Liu, R., He, X., Gao, Z., Tao, L., Zhou, X., and Zhang, L., 2018, A Late Mesozoic short-lived shift from fluid-dominated to sediment-dominated mantle metasomatism in the northeast South China Block and its tectonic implications: Lithos, v. 310, p. 288–301, https://doi.org/10.1016/j.lithos.2018.04.019.

Pan, X., Shen, Z., Roberts, A.P., Heslop, D., and Shi, L., 2014, Syntectonic emplacement of Late Cretaceous mafic dyke swarms in coastal southeastern China: Insights from magnetic fabrics, rock magnetism and field evidence: Tectonophysics, v. 637, p. 328–340, https://doi.org/10.1016/j.tecto.2014.10.018.

Pitcher, W.S., 1983, Granite type and tectonic environment, in Hsu K., ed., Mountain Building Processes: London, UK, Academic Press, p. 19–40.

Qi, Y., Hu, R., Liu, S., Coulson, I.M., Qi, H., Tian, J., and Zhu, J., 2016, Petrogenesis and geodynamic setting of Early Cretaceous mafic-ultramafic intrusions, South China: A case study from the Gan-Hang tectonic belt: Lithos, v. 258–259, p. 149–162, https://doi.org/10.1016/j.lithos.2016.04.027.

Qiu, J., Wang, D., McInnes, B.I.A., Jiang, S., and Wang, R., 2004, Two subgroups of A-type granites in the coastal area of Zhejiang and Fujian provinces, SE China: Age

and geochemical constraints on their petrogenesis: Transactions of the Royal Society of Edinburgh. Earth Sciences, v. 95, p. 227–236, https://doi.org/10.1017/S0263593300001036.

Qiu, Y.M., Shan, G., McNaughton, N.J., Groves, D.I., and Ling, W., 2000, First evidence of >3.2 Ga continental crust in the Yangtze craton of south China and its implications for Archean crustal evolution and Phanerozoic tectonics: Geology, v. 28, p. 11, https://doi.org/10.1130/0091-7613(2000)028<0011:FEOGCC>2.0.CO;2.

Rapp, R.P., and Watson, E.B., 1995, Dehydration melting of metabasalt at 8–32 kbar: Implications for continental growth and crust-mantle recycling: Journal of Petrology, v. 36, p. 891–931, https://doi.org/10.1093/petrology/36.4.891.

Schellart, W.P., Lister, G.S., and Toy, V.G., 2006, A Late Cretaceous and Cenozoic reconstruction of the Southwest Pacific region: Tectonics controlled by subduction and slab rollback processes: Earth-Science Reviews, v. 76, p. 191–233, https://doi.org/10.1016/j.earscirev.2006.01.002.

Scherer, E., Munker, C., and Mezger, K., 2001, Calibration of the lutetium-hafnium clock: Science, v. 293, p. 683–687, https://doi.org/10.1126/science.1061372.

Sdrolias, M., and Müller, R.D., 2006, Controls on back-arc basin formation: Geochemistry, Geophysics, Geosystems, v. 7, no. 4, https://doi.org/10.1029/2005GC001090.

Sdrolias, M., Roest, W.R., and Müller, R.D., 2004, An expression of Philippine Sea plate rotation: The Parece Vela and Shikoku Basins: Tectonophysics, v. 394, p. 69–86, https://doi.org/10.1016/j.tecto.2004.07.061.

Shen, W., Ling, H., Wang, D., Xu, B., and Yu, Y., 1999, Study on Nd-Sr isotopes of Mesozoic igneous rocks in Zhejiang, China [in Chinese with English abstract]: Scientia Geologica Sinica, v. 34, p. 223–232.

Shui, T., 1988, Tectonic framework of the continental basement of southeast China [in Chinese with English abstract]: Science China. Chemistry, v. 31, p. 885–896.

Sibuet, J., and Hsu, S., 1997, Geodynamics of the Taiwan arc-arc collision: Tectonophysics, v. 274, p. 221–251, https://doi.org/10.1016/S0040-1951(96)00305-8.

Sisson, T.W., Ratajeski, K., Hankins, W.B., and Glazner, A.F., 2005, Voluminous granitic magmas from common basaltic sources: Contributions to Mineralogy and Petrology, v. 148, p. 635–661, https://doi.org/10.1007/s00410-004-0632-9.

Sun, F., Xu, X., Zou, H., and Yan, X., 2015, Petrogenesis and magmatic evolution of ~130 Ma A-type granites in Southeast China: Journal of Asian Earth Sciences, v. 98, p. 209–224, https://doi.org/10.1016/j.jseaes.2014.11.018.

Sun, S.S., and McDonough, W.F., 1989, Chemical and isotopic systematics of oceanic basalts: Implications for mantle composition and processes, *in* Saunders, A.D., and Norry, M.J., eds., Magmatism in the Ocean Basin: Geological Society of London, Special Publication 42, p. 313–345, https://doi.org/10.1144/GSL.SP.1989.042.01.19.

Tang, Z.C., Dong, X.F., Wen-Jie, H.U., Meng, X.S., and Rong, Y.P., 2014, SHRIMP zircon U-Pb dating of Xianlin granodiorite rock in western Zhejiang and their geological significance [in Chinese with English abstract]: Geoscience, v. 28, p. 884–892.

Tchameni, R., Mezger, K., Nsifa, N.E., and Pouclet, A., 2001, Crustal origin of Early Proterozoic syenites in the Congo Craton (Ntem Complex): South Cameroon: Lithos, v. 57, p. 23–42, https://doi.org/10.1016/S0024-4937(00)00072-4.

Tiepolo, M., Oberti, R., and Vannucci, R., 2002, Trace-element incorporation in titanite: Constraints from experimentally determined solid/liquid partition coefficients: Chemical Geology, v. 191, p. 105–119, https://doi.org/10.1016/S0009-2541(02)00151-1.

Turner, S.P., Foden, J.D., and Morrison, R.S., 1992, Derivation of some A-type magmas by fractionation of basaltic magma: An example from the Padthaway Ridge, South Australia: Lithos, v. 28, p. 151–179, https://doi.org/10.1016/0024-4937(92)90029-X.

Wang, Z., Wang, J., Du, Q., Deng, Q., and Yang, F., 2013, The evolution of the Central Yangtze Block during early Neoarchean time: Evidence from geochronology and geochemistry: Journal of Asian Earth Sciences, v. 77, p. 31–44, https://doi.org/10.1016/j.jseaes.2013.08.013.

Watson, E.B., and Harrison, T.M., 1983, Zircon saturation revisited: Temperature and composition effects in a variety of crustal magma types: Earth and Planetary Science Letters, v. 64, no. 2, p. 295–304, https://doi.org/10.1016/0012-821X(83)90211-X.

Whalen, J.B., 1985, Geochemistry of an island-arc plutonic suite: The Uasilau-Yau Yau intrusive complex, New Britain, P.N.G: Journal of Petrology, v. 26, p. 603–632, https://doi.org/10.1093/petrology/26.3.603.

Whalen, J.B., Currie, K.L., and Chappell, B.W., 1987, A-type granites: Geochemical characteristics, discrimination and petrogenesis: Contributions to Mineralogy and Petrology, v. 95, p. 407–419, https://doi.org/10.1007/BF00402202.

Wiedenbeck, M., Alle, P., Corfu, F., Griffin, W.L., Meier, M., Oberli, F., Quadt, A.V., Roddick, J.C., Spiegel, W., and Oberli, F.V.Q.A., 1995, Three natural zircon standards for U-Th-Pb, Lu-Hf, trace element and REE analyses: Geostandards Newsletter, v. 19, p. 1–23, https://doi.org/10.1111/j.1751-908X.1995.tb00147.x.

Wong, J., Sun, M., Xing, G., Li, X., Zhao, G., Wong, K., Yuan, C., Xia, X., Li, L., and Wu, F., 2009, Geochemical and zircon U-Pb and Hf isotopic study of the Baijuhuajian metaluminous A-type granite: Extension at 125–100?Ma and its tectonic significance for South China: Lithos, v. 112, p. 289–305, https://doi.org/10.1016/j.lithos.2009.03.009.

Xiao, W., and He, H., 2005, Early Mesozoic thrust tectonics of the northwest Zhejiang region (Southeast China): Geological Society of America Bulletin, v. 117, p. 945–961, https://doi.org/10.1130/B25417.1.

Xie, L., Wang, D.Z., Wang, R.C., Qui, J.X., and Chen, X.M., 2004, Complex zoning texture in plagioclases from the quartz diorite enclave in the Putuo granitic complex, Zhejiang province: record of magma mixing [in Chinese with English abstract]: Yanshi Xuebao, v. 20, p. 1397–1408.

Xu, X.S., O'Reilly, S.Y., Zhou, X.M., and Griffin, W.L., 1996, A xenolith-derived geotherm and the crust-mantle boundary at Qilin, southeastern China: Lithos, v. 38, p. 41–62, https://doi.org/10.1016/0024-4937(95)00043-7.

Xu, X., Dong, C., Li, W., and Zhou, X., 1999, Late Mesozoic intrusive complexes in the coastal area of Fujian, SE China: The significance of the gabbro-diorite granite association: Lithos, v. 46, p. 299–315, https://doi.org/10.1016/S0024-4937(98)00087-5.

Xu, X., O'Reilly S. Y., Griffin W. L., Deng P. and Pearson N. J., 2005, Relict Proterozoic basement in the Nanling Mountains (SE China) and its tectonothermal overprinting: Tectonics, v. 24, https://doi.org/10.1029/2004TC001652.

Xu, X., Reilly, S.Y.O., Griffin, W.L., Wang, X., Pearson, N.J., and He, Z., 2007, The crust of Cathaysia: Age, assembly and reworking of two terranes: Precambrian Research, v. 158, p. 51–78, https://doi.org/10.1016/j.precamres.2007.04.010.

Yang, J., Wu, F., Chung, S., Wilde, S.A., and Chu, M., 2006, A hybrid origin for the Qianshan A-type granite, northeast China: Geochemical and Sr-Nd-Hf isotopic evidence: Lithos, v. 89, p. 89–106, https://doi.org/10.1016/j.lithos.2005.10.002.

Yang, S.Y., Jiang, S., Zhao, K., Jiang, Y., Ling, H., and Luo, L., 2012, Geochronology, geochemistry and tectonic significance of two Early Cretaceous A-type granites in the Gan-Hang Belt, Southeast China: Lithos, v. 150, p. 155–170, https://doi.org/10.1016/j.lithos.2012.01.028.

Yang, Z.L., Shen, W.Z., Tao, K.Y., and Shen, J.L., 1999, Sr, Nd and Pb isotopic characteristics of early Cretaceous basaltic rocks from the coast of Zhejiang and Fujian: Evidences for ancient enriched mantle source [in Chinese with English abstract]: Scientia Geologica Sinica, v. 34, p. 59–68.

Yu, J.H., Reilly, S.Y.O., Zhou, M., Griffin, W.L., and Wang, L., 2012, U-Pb geochronology and Hf-Nd isotopic geochemistry of the Badu Complex, Southeastern China: Implications for the Precambrian crustal evolution and paleogeography of the Cathaysia Block: Precambrian Research, v. 222–223, p. 424–449, https://doi.org/10.1016/j.precamres.2011.07.014.

Yu, Y.W., Zhou, T.X., and Chen, J.F., 1993, The characteristics and origin of Xuantandi bimodal volcanic rocks of the late stages of early Cretaceous, Zhejiang [Earth Science]: Journal of Nanjing University, v. 5, p. 420–429.

Zhang, B.T., and Zhang, Z.H., 1993, The evolution of continental crust and uranium metallization in Southeastern China [in Chinese]: Beijing, China, Atomic Energy Press, 77–94 p.

Zhang, J.B., Liu, Y.S., Ling, W.L., and Gao, S., 2017, Pressure-dependent compatibility of iron in garnet: Insights into the origin of ferropicritic melt: Geochimica et Cosmochimica Acta, v. 197, p. 356–377, https://doi.org/10.1016/j.gca.2016.10.047.

Zhang, X.L., Qiu, J.S., Wang, D.Z., Wang, R.C., Xi-Sheng, X.U., and Chen, X.M., 2005, Geochemistry and magmatic mixing of the Putuoshan biotite moyites and their enclaves [in Chinese with English abstract]: Zhejiang Province: Acta Petrologica Et Mineralogica, v. 24, p. 81–92.

Zhao, J.L., Qiu, J.S., Liu, L., and Wang, R.Q., 2016, The Late Cretaceous I- and A-type granite association of southeast China: Implications for the origin and evolution of post-collisional extensional magmatism: Lithos, v. 240–243, p. 16–33, https://doi.org/10.1016/j.lithos.2015.10.018.

Zhao, L., Zhou, X., Zhai, M., Santosh, M., Ma, X., Shan, H., and Cui, X., 2014, Paleoproterozoic tectonic transition from collision to extension in the eastern Cathaysia Block, South China: Evidence from geochemistry, zircon U-Pb geochronology and Nd-Hf isotopes of a granite-charnockite suite in southwestern Zhejiang: Lithos, v. 184–187, p. 259–280, https://doi.org/10.1016/j.lithos.2013.11.005.

Zhao, L., Zhou, X., Zhai, M., Santosh, M., and Geng, Y., 2015, Zircon U-Th-Pb-Hf isotopes of the basement rocks in northeastern Cathaysia block, South China: Implications for Phanerozoic multiple metamorphic reworking of a Paleoproterozoic terrane: Gondwana Research, v. 28, p. 246–261, https://doi.org/10.1016/j.gr.2014.03.019.

Zheng, J., Griffin, W.L., O'Reilly, S.Y., Zhang, M., Pearson, N., and Pan, Y., 2006, Widespread Archean basement beneath the Yangtze craton: Geology, v. 34, p. 417–420, https://doi.org/10.1130/G22282.1.

Zhou, X.M., and Li, W.X., 2000, Origin of Late Mesozoic igneous rocks in Southeastern China: Implications for lithosphere subduction and underplating of mafic magmas: Tectonophysics, v. 326, p. 269–287, https://doi.org/10.1016/S0040-1951(00)00120-7.

Zhou, X., Sun, T., Shen, W., Shu, L., and Niu, Y., 2006, Petrogenesis of Mesozoic granitoids and volcanic rocks in South China: A response to tectonic evolution: Episodes, v. 29, p. 26–33, https://doi.org/10.18814/epiiugs/2006/v29i1/004.

Science Editor: Bradley S. Singer
Associate Editor: Nicholas Timms

Manuscript Received 13 July 2019
Revised Manuscript Received 12 September 2019
Manuscript Accepted 18 October 2019

Printed in the USA